BOOK OF ABSTRACTS

IMAM 2025

INTERNATIONAL MEETING ON ADVANCED MATERIALS

10TH -12TH MARCH 2025, JASNÁ, SLOVAKIA

Organized by

Supported by

Pavol Jozef Šafárik University in Košice

BOOK OF ABSTRACTS

International Meeting on Advanced Materials

March 10-12, 2025

Organized by:

Slovak Chemical Society
&
Slovak Academy of Sciences

Košice 2025

Edited by: Mgr. Soňa Király, *Institute of Chemistry, Pavol Jozef Šafárik University in Košice, Moyzesova 11, 040 01 Košice, Slovakia, sona.kiraly@upjs.sk*

Reviewed by: Prof. Dr. Ayşegül Öksüz, *Faculty of Engineering and Natural Sciences, Suleyman Demirel University, Çünür, Süleyman Demirel Cd., 32260 Merkez/Isparta, Turkey, ayseguluygun@sdu.edu.tr*

Dr. Kadir Özaltin, *Centre of Polymer Systems, Tomas Bata University in Zlín, 760 01 Zlín, Czech Republic, ozaltin@utb.cz*

Organized by:

Slovak Chemical Society

Slovak Academy of Sciences

Available at: www.unibook.upjs.sk

Publication date: 02.04.2025

ISBN 978-80-574-0396-8 (e-publication)

LIST OF CONTENTS

LIST OF AUTHORS

Preface

On behalf of the IMAM 2025 Organizing Committee, it is our pleasure to present these proceedings, which compile the contributions from the **International Meeting on Advanced Materials (IMAM)**, held on **10–12 March 2025** in **Jasná, Slovakia**. This conference is organized by the **Slovak Chemical Society** in cooperation with the **Slovak Academy of Sciences**

IMAM 2025 provides a platform for researchers working in the field of advanced materials to share their latest findings, discuss innovative approaches, and explore emerging trends in materials science. The primary objective of the meeting is to promote scientific exchange across a broad spectrum of topics related to advanced materials and to foster new collaborations within the international research community.

These proceedings include the full texts of the oral contributions presented at the conference. We hope that this collection offers readers a valuable overview of the diverse and significant topics addressed during the meeting.

We sincerely thank all authors for submitting their latest research and thereby contributing to the high scientific quality of the conference. Special appreciation is also extended to the reviewers for their careful evaluation of the submitted papers and to the entire organizing team for their dedication in ensuring the success of IMAM 2025.

We wish all participants an inspiring and productive scientific meeting in **Low Tatras area at Hotel Damian** and hope that IMAM 2025 will serve as a valuable opportunity to gain new insights and foster future collaborations in the field of advanced materials.

Soňa Király

Lectures

Electrochemical Sensor Modified by Metal-Organic Frameworks for Ciprofloxacin Detection

R. Oriňaková[a,*], J. Demeterová [a], N. Király [b], S. Király [a], J. Shepa[a], I. Šišoláková[a]

[a]Department of Physical Chemistry, University of P. J. Šafárik in Košice, Moyzesova 11, 040 01 Košice, Slovak Republic

[b]Department of Inorganic Chemistry, University of P. J. Šafárik in Košice, Moyzesova 11, 040 01 Košice, Slovak Republic

[*]renata.orinakova@upjs.sk

A common antibiotic used to treat bacterial infectious diseases in humans, animals, and poultry is ciprofloxacin (CIP). Typhoid fever (enteric fever), respiratory, urinary, chronic bronchitis, gastrointestinal, eye, and skin infections are the main conditions for which it is prescribed. As a treatment for both gram-positive and gram-negative bacteria, CIP is also frequently prescribed. Because CIP can be taken orally as well as through parental mode, it can be used to treat a wide range of infectious diseases. However, improper administration of CIP dosages can lead to adverse effects like diarrhea, allergies, liver function changes, headaches, nausea, and vomiting [1]. There are a number of methods dealing with the separation and/or the quantification of antibiotics among them immunological, ultraviolet methods, gas chromatography, liquid chromatography etc. [2]. All of the above methods are time-consuming, expensive, and require trained personnel. Furthermore, real-time or bed-site detection is not possible.

Electrochemical detection of antibiotics overcome these drawbacks. Moreover, the screen-printed electrodes (SPCE) ensure miniaturisation and lower sample consumption. SPCE electrodes modified by metal-organic frameworks (MOFs) have been used for antibiotics detection [3], [4], [5].

MOFs are hybrid inorganic-organic porous coordination polymers made up of organic linkers and metal nodes. Metal cations frequently group together to create clusters with distinctive secondary building units of various shapes. There are currently about 80 known elements that can function as central atoms and even more organic ligands. They can be combined to create an infinite number of MOF compounds with adjustable pore size and design [6]. Due to their large surface area, rich chemical tunability, active metal sites, and homogenous porous structure, MOFs have been thoroughly studied in a variety of fields, including gas storage and separation, sensors, and catalysis [3].

Herein, ciprofloxacin was detected in PBS solution using SPCE-MOF electrodes. A carbon working electrode, an Ag/AgCl pseudoreference electrode, and a carbon counter electrode are the three electrodes that make up the screen-printed carbon electrode (SPCE 11L, Metrohm DropSens), which is printed on a ceramic plate. A metal-organic framework (MOF) was used to enhance properties of the carbon working electrode. In order to accomplish this, 1 µl of MOF suspension in a 1:1 mixture of absolute ethanol and water was applied to the working electrode surface and allowed to air dry for 10 minutes at room temperature.

The modified electrodes were characterized by scanning electron microscopy SEM/FIB ZEISS AURIGA. Cyclic voltammetry (CV) was also used to determine the amount of ciprofloxacin in the solution. Using a potentiostat (Metrohm Autolab PGSTAT302N, Switzerland) with a potential range of 0 V to 1.5 V and a scan rate of 100 mV/s, measurements were made. For antibiotic detection, a 1 mM ciprofloxacin solution was prepared in PBS and subsequently diluted to concentrations of 0.8, 0.6, 0.4, 0.2, 0.1, 0.08, 0.06, 0.04, 0.02, and 0.01 mM. Then, 60 µl of each antibiotic concentration was dropped onto the MOF-modified working electrode and measured using CV.

Surface morphology of SPCE electrodes was studies via scanning electron microscopy. SPCE display rough surface consisting of sheets of carbon material. SPCE working electrode surface was modified by MOF via drop-casting method. As shown in the Fig. 1, MOF was in-homogeneously dispersed on the working electrode surface. Moreover, the MOF crystals had different shape and size.

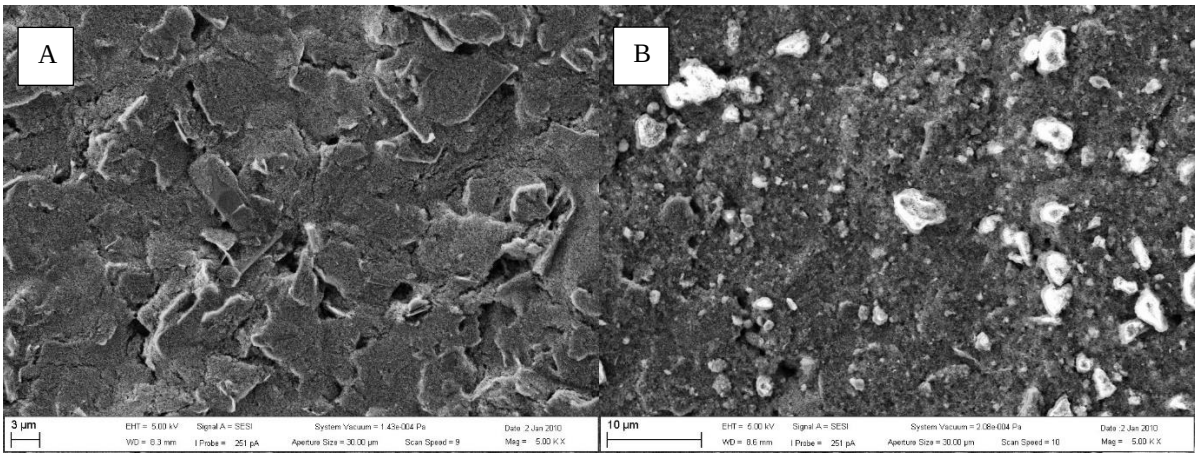

Fig. 1: SEM images for SPCE (scale – 3 µm, mag 5.00 KX; A) and SPCE-MOF (scale – 10 µm, mag 5.00 KX; B).

Cyclic voltammetry was used for ciprofloxacin detection within the concentration windows from 10 µM to 1000µM. Cyclic voltammograms for ciprofloxacin displays 1 oxidation peak and none reduction peak which indicated irreversible electrochemical reaction. This behaviour is typical for various organic biomolecules. Dependence of current on concentration of ciprofloxacin (Fig. 2, inset**)** was fitted by linear function. The calculated sensitivity was 2.77 nA/µM and limit of detection was 134 µM.

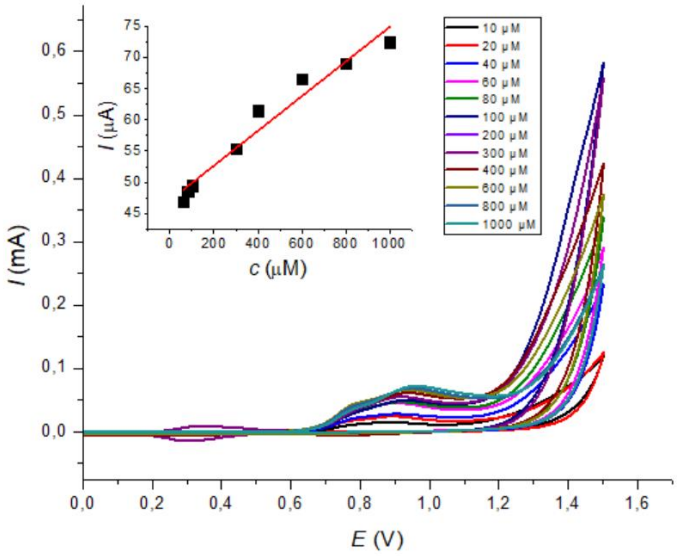

Fig. 2: Cyclic voltammograms for various concentrations of ciprofloxacin on SPCE-MOF. Calibration curve (inset).

Based on the wide concentration range the SCPE modified by MOF, proposed electrode is a promising candidate for future detection of ciprofloxacin in the real samples.

Acknowledgements

This work was funded by the EU NextGenerationEU through the Recovery and Resilience Plan for Slovakia under the project No. 09-I05-03-V02-00047.

References

[1] M. A. Khaleque, M. R. Ali, M. A. S. Aly, M. I. Hossain, K. H. Tan, M. A. Zaed, R. Saidur, M. M. Rahman, N. M. Mubarak, M. Z. H. Khan, "Highly sensitive electrochemical detection of ciprofloxacin using MXene ($Ti_3C_2T_x$)/poly (rutin) composite as an electrode material," *Diam Relat Mater*, vol. 150, Dec. 2024, doi: 10.1016/j.diamond.2024.111749.

[2] I. T. Somé, R. Semde, O. Moustapha, K. Amighi, P. I. Guissou, P. Duez, J. Dubois, "Validation of gentamicin congeners using HPLC with electrochemical detection: Comparison with fluorimetric detection," *Comptes Rendus Chimie*, vol. 7, no. 10–11, pp. 1087–1093, Oct. 2004, doi: 10.1016/j.crci.2003.12.037.

[3] N. M. Umesh, J. Antolin Jesila, S. F. Wang, N. Vishnu, and Y. J. Yang, "Novel voltammetric detection of norfloxacin in urine and blood serum using a flexible Ni foam based Ni-Co-MOF ultrathin nanosheets derived from Ni-Co-LDH," *Microchemical Journal*, vol. 160, Jan. 2021, doi: 10.1016/j.microc.2020.105747.

[4] A. D. Ambaye, M. Muchindu, A. Jijana, S. Mishra, and E. Nxumalo, "Screen-printed electrode system based on carbon black/copper-organic framework hybrid nanocomposites for the electrochemical detection of nitrite," *Mater Today Commun*, vol. 35, Jun. 2023, doi: 10.1016/j.mtcomm.2023.105567.

[5] A. D. Ambaye, T. G. Kebede, B. Ntsendwana, and E. N. Nxumalo, "Fe-MOF derived graphitic carbon nitride nanocomposites as novel electrode materials for the electrochemical sensing of 2,4-dichlorophenol in wastewater," *Synth Met*, vol. 299, Nov. 2023, doi: 10.1016/j.synthmet.2023.117452.

[6] M. Almáši, "Current development in MOFs for hydrogen storage," in *Metal-Organic Framework-Based Nanomaterials for Energy Conversion and Storage*, Elsevier, 2022, pp. 631–661. doi: 10.1016/b978-0-323-91179-5.00020-6.

Li-ion and Redox Flow Batteries for Hybrid Energy Storage Systems – Recent Developments, Models and Simulations

A. S. Fedorková[a*], N. Podrojková[a], V. Niščáková[a], M. Almáši[a], J. A.-Pascual[b], E. Romadina[b]

[a]Institute of Chemistry, Faculty of Science, P. J. Šafárik University, Moyzesova 11, 041 54 Košice, Slovakia

[b]INO-HUB Energy, Tomášikova 30, 821 01 Bratislava, Slovakia

[*]andrea.fedorkova@upjs.sk

Keywords: Li-ion batteries, Li-S batteries, MOF, redox-flow batteries, applied research

Introduction

The advancement of energy storage technologies, particularly lithium-ion batteries (LiBS) and redox flow batteries (RFBs), is crucial for supporting the global transition to renewable energy sources. Recent applied research has focused on developing novel materials, employing advanced modelling techniques, and conducting rigorous testing to enhance the performance, safety, and cost-effectiveness of these batteries. An essential factor in their acceptance is durability and the use of ethically sourced materials, minimizing environmental harm. Ensuring these batteries can be efficiently recycled or repurposed at the end of their lifecycle is key to returning valuable materials to the economy.

So far, lithium-ion batteries have dominated the secondary battery market, widely used in electric mobility, portable electronic devices, and energy storage systems due to their high energy density, stability, and proven performance. However, continued innovation in LIBs is expected, particularly in electrode materials, electrolytes, separators, and cell structures. Alongside LIBs, RFBs (Fig. 1) are emerging as leading technology for grid-scale stationary energy storage. Their ability to store large amounts of electrical energy for long durations and release it quickly when needed, combined with their long lifespan and solid efficiency, makes them highly attractive. In RFBs, the redox couples and electrolytes are crucial in determining energy density and overall cost. This study focuses on developing a novel battery component through advanced modelling and lab testing of different components for Li-S and redox flow batteries.

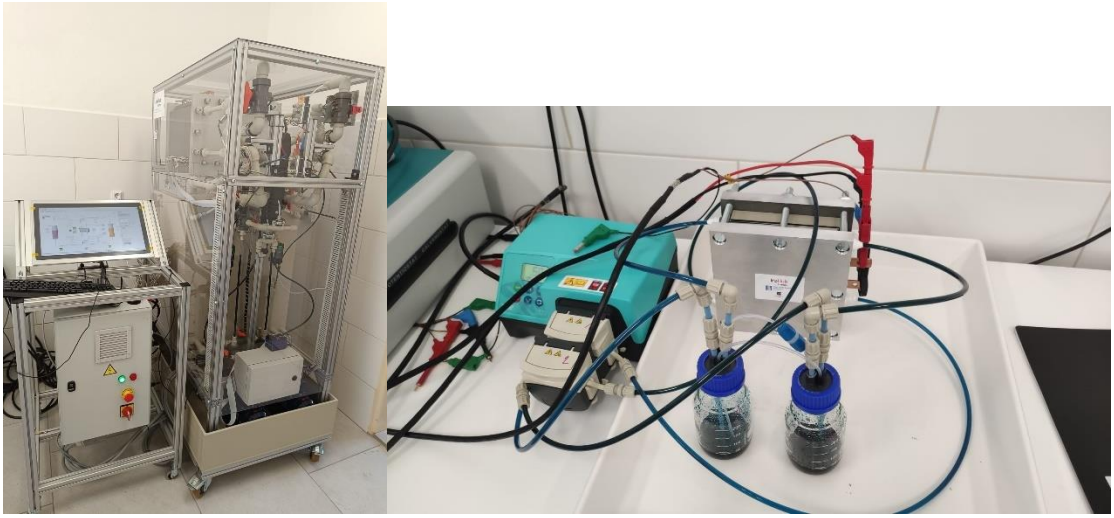

Fig. 1 Redox flow battery testing rig and single cell for testing of battery components.

Novel Materials for Li-ion and Li-S Batteries

Researchers are exploring innovative materials for Li-ion batteries to improve their energy density, lifespan, and safety. For instance, alternative electrode materials such as oxides, MOFs, phosphates, and sulphides are being investigated to enhance battery capacity and safety. Additionally, the development of solid-state electrolytes aims to replace conventional liquid electrolytes, potentially reducing flammability and increasing energy density. These advancements are highlighted in a special issue focusing on novel materials for Li-ion batteries.

MOF STAM-1 with unique structure (hexagonal hydrophobic and trigonal hydrophilic pores) was used as a cathode material for Li-S batteries. This structure is stabilizing and improving the properties of Li-S cathode, such as volumetric expansion of sulfur during cycling or polysulfide trapping, which prevented the polysulfide shuttle effect. STAM-1 successfully encapsulated sulfur in the pores, thereby improving the electrochemical activity of the cathode. In addition, the catalytic effect of copper and improved redox kinetics of sulfur cathodes were confirmed. The initial discharge capacity of this cathode (S/STAM-1/Super P/PVDF) was 495 mAh/g at a rate of 0.2 C (Fig. 2). The initial discharge capacity at a rate of 0.5 C was 452 mAh/g and after one hundred cycles was 430 mAh/g, with a Coulombic efficiency of 97% during all cycles at 0.5 C. These results confirmed that STAM-1 is a promising host material for a sulfur cathode in a Li–S battery. Furthermore, the combination of bimodal structure and pore size with the use of Lewis acid is the best combination to create a novel MOF-based cathode material with improved stability and performance.

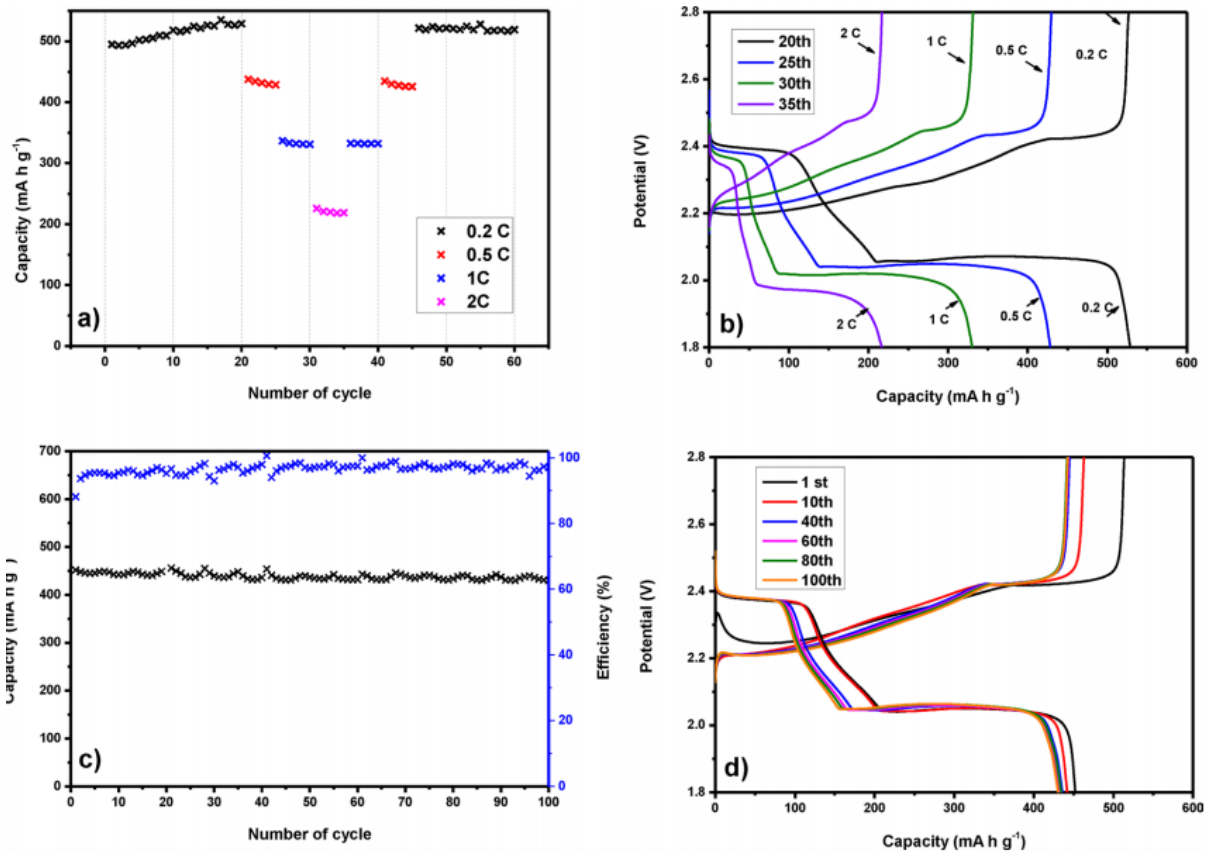

Fig. 2 Electrochemical characteristics during cycling for the electrode containing STAM-1.

Modelling and Simulation in Battery Development

Computational modelling plays a pivotal role in understanding and predicting battery behaviour, thereby accelerating the development of new materials. For Li-ion batteries, atomistic simulation software like Synopsys QuantumATK enables the design of novel materials for various components, including cathodes, anodes, and electrolytes. This approach allows for systematic selection and optimization of materials, reducing development time and costs. In the realm of RFBs, machine learning (ML) integrated with high-throughput computational screening (HTCS) has been instrumental in discovering and optimizing materials. This integration facilitates the rapid identification of suitable redox-active materials, enhancing the efficiency and cost-effectiveness of RFBs. RFBs have emerged as promising candidates for large-scale energy storage due to their scalability and flexibility. Recent studies have focused on developing non-aqueous RFBs that operate over a wider voltage range, achieving high efficiency and prolonged cycle life. For example, a prototype utilizing a specific redox pair demonstrated a discharge cell voltage ranging from approximately 2.25 V to 1.9 V [1]. To evaluate the scalability of this design, a two-dimensional time-transient reactive transport model was developed, accurately predicting voltage behaviour and providing insights into species transport within the cell.

From the physical point of view, the model was defined using laminar flow in the case of channels without felt. In the case of channels with felt, the model was defined using laminar flow and porous medium (Fig. 3). The flow rate was

set to 1/min. The resulting values showed the need to reconsider the definition of the physics of the system, where the Kozeny-Carman equation was used, which may not be suitable for defining the system under consideration and the system can be defined in another way. In addition, the electrolyte permeability value must be experimentally determined or determined by simulations using the inlet pressure values obtained from experimental measurements.

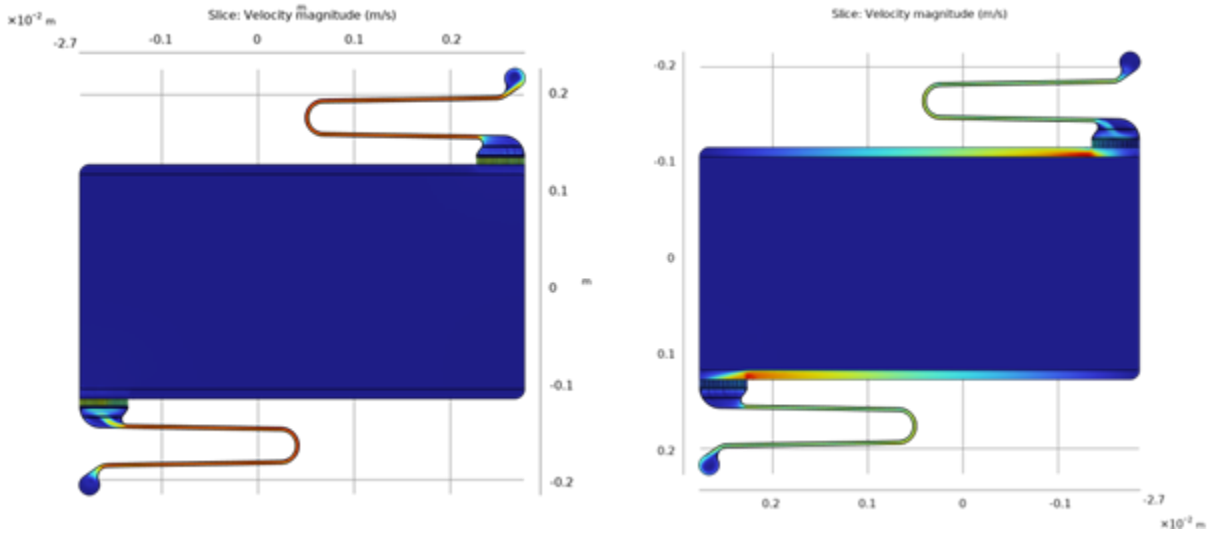

Fig. 3 Results of simulations of electrolyte flow in channels for determining pressure loss.

Conclusion

A series of new porous structures based on HEO and MOF with a micro/nano porous structure were developed. These materials are suitable for sulphur and polysulfides trapping and allows fast electron transfer, long cycling and lower volume expansion. Instead of PVDF, we applied new binders and additives with self-healing effect such as carrageenan or polypyrrole [2]. These materials are ecological, cheap and do not require the use of expensive solvents such as NMP. The results of these experiments confirmed the improvement of cyclability and stability and the possibility of using these materials in practice. Novel materials based on MOF structures for Li-S batteries were prepared and tested where the initial discharge capacity was 495 mAh/g at a rate of 0.2 C. Advanced modelling and testing of redox flow batteries is driving significant improvements in efficiency and stability of novel components. These advancements are essential for meeting the growing energy demands and facilitating the integration of renewable energy sources into the grid.

Acknowledgments

This work was funded by the project APVV-20-0111, project KEGA 002UPJŠ-4/2024, by the Recovery and Resilience Plan for Slovakia under the project SUNFLOWERS no. 09I02-03-V01-00022 and by the project IPCEI_IE_FLOW_BESS_012021.

References

[1] D. Xu, C. Zhang, Y. Zhen, Y. Zhao, Y. Li, "A high-rate nonaqueous organic redox flow battery", *J. Power Sources*, vol. 495, 2021, 229819, doi: 10.1016/j.jpowsour.2021.229819.

[2] D. Zalka, A. Vizintin, A. Maximenko, Z. Pászti, Z. Dankházi, K. Hegedüs, L.S. Shankar, R. Kun, K. Saksl, A. Straková Fedorková, P. Jóvári, „Improving lithium-sulfur battery performance using a polysaccharide binder derived from red algae", *Comm. Mat*., 6 (1), art. no. 17, 2025, doi: 10.1038/s43246-025-00734-1.

Characterization of Carbon Recycled Materials via RAMAN and XRF Analysis

I. Šišoláková[a]*, N. Jašňáková[a], O. Petruš[b], J. Shepa[a], J. Jaščišák[c], R. Oriňaková[a,d]

[a]Department of Physical Chemistry, Faculty of Science, Pavol Jozef Šafárik University in Košice, Moyzesová 11, 040 01, Košice, Slovak Republic

[b]Institute of Materials Research, Slovak Academy of Sciences, Watsonova 47, 040 01 Kosice, Slovak Republic

[c]Fecupral, spol. s r.o., Jilemnického 3578, 080 01 Prešov, Slovak republic

[d]Centre of Polymer Systems, Tomáš Baťa University in Zlín, Třída Tomáše Bati 5678, 760 01, Zlín, Czech Republic

*ivana.sisolakova@upjs.sk

The growing prevalence of diabetes has intensified the need for reliable, cost-effective, and sensitive methods for monitoring glucose and insulin levels. Traditional insulin detection methods, including enzyme-linked immunosorbent assays (ELISA) and liquid chromatography, are often expensive, time-consuming, and require specialized equipment. In contrast, electrochemical sensors have gained significant attention as potential tools for the rapid, on-site, and affordable detection of insulin levels, offering real-time monitoring with high sensitivity and specificity.

A key challenge in developing electrochemical sensors is the need for advanced materials that can enhance the sensors' sensitivity, stability, and reproducibility. Recent research has focused on utilizing carbon-based materials due to their excellent electrical conductivity, leading to current response increasement in sensor applications. Carbon materials, in combination with metal particles, mainly nickel, which ensures the selectivity of insulin electrochemical sensors, can be considered an ideal electrode modification for future insulin sensor development.

However, developing these materials often relies on costly and environmentally taxing processes. Considering these challenges, carbon waste materials have emerged as promising alternatives. The use of waste-derived carbon materials, such as those from agricultural residues, industrial by-products, and municipal waste, offers an innovative solution for creating sustainable, cost-effective sensor platforms. These materials can be engineered to possess the required electrochemical properties for insulin detection, providing an environmentally friendly and economical approach to sensor fabrication. Furthermore, utilizing waste carbon materials aligns with the principles of circular economy, helping to reduce the environmental impact while promoting resource efficiency.

In this study, we explore the elemental composition of carbon recycled powders derived from secondary waste processes (Fecupral, Slovakia), doped with various metals (Cu, Ni, Zn, etc.) via Raman spectroscopy and X-ray fluorescence (XRF). Five carbon waste samples (A-E) were tested to find those with the most suitable elemental composition containing the highest amount of Ni, which is essential for insulin oxidation. Based on the obtained results, the best sample for future modification of the screen-printed electrode (SPCE) for insulin determination was chosen. Due to the XRF analysis as the most suitable samples can be considered samples B and C with 32.60 and 34.46% of Ni, respectively.

Thereafter, the Raman spectra of all five samples (A-E) were done. The Raman spectrum of graphite exhibits three characteristic peaks: the D-band (~1350 cm^{-1}), G-band (~1580 cm^{-1}), and 2D-band (~2700 cm^{-1}). The G-band corresponds to the in-plane vibrations of sp^2 carbon atoms, while the D-band appears due to structural defects and disorder. The 2D-band is the second-order overtone of the D-band. Additional peaks observed at 650 cm^{-1} and 690 cm^{-1} may be related to defect-induced vibrational modes, oxygen-containing functional groups, or trace metal impurities.

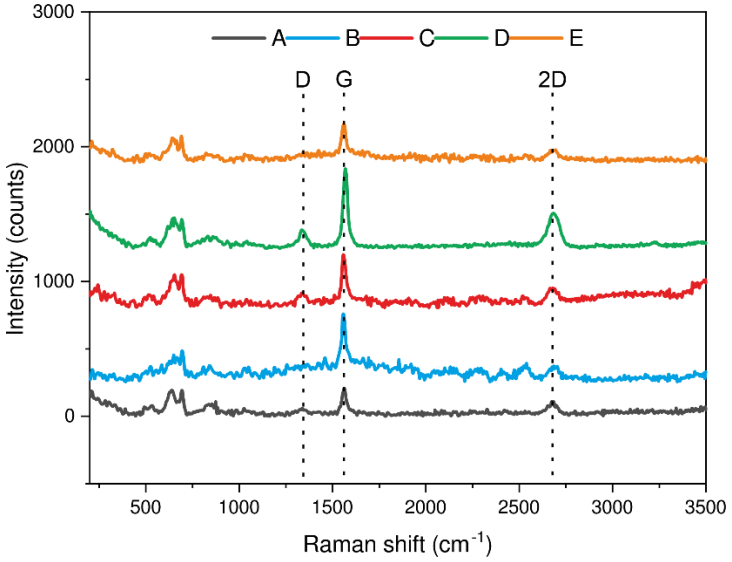

Fig. 1: Raman spectra of various carbon-based waste materials (A-E)

In conclusion, this study demonstrated the potential of carbon waste materials as effective electrode components for insulin sensing. Among the tested samples, Sample B and Sample C exhibited superior performance due to their higher Ni content, which is crucial for insulin oxidation. These findings highlight the importance of Ni incorporation in sensor development and suggest that optimized carbon waste materials could serve as sustainable and efficient alternatives for electrochemical insulin detection.

Acknowledgements

Funded by the EU NextGenerationEU through the Recovery and Resilience Plan for Slovakia under the project No. 09I03-03-V04-00180.

Electrochemically Deposited Ceramic Coatings on Zinc Foam Substrates: Initial Steps Toward Deposition Optimization

R. Gorejová[a]*, I. Mojžišová[a], C. Wiener[b], R. Oriňaková[a]

[a]Department of Physical Chemistry, Faculty of Science, P.J. Šafárik University in Košice, Moyzesova 11, 041 54, Košice, Slovakia

[b]Department of Materials Science and Engineering, Budapest University of Technology and Economics, Műegyetem rkp. 3., H-1111 Budapest, Hungary

*radka.gorejova@upjs.sk

Introduction

In the field of biodegradable material development, zinc is emerging as a promising alternative to traditionally used metals [1]. Its favourable biological properties and crucial role in bone tissue regeneration make it a strong candidate for biomedical applications. However, like other metals in this domain, zinc exhibits certain limitations, including insufficient mechanical strength and localized toxicity, particularly in the early post-implantation period.

To address these challenges, various approaches are being explored, such as zinc alloys and specific structural designs [2,3]. In this study, we focused on the surface modification of zinc-based materials to mitigate the uncontrolled release of Zn^{2+} ions, which can lead to acute toxicity in the surrounding implant environment [4]. A hydroxyapatite ceramic coating was selected as the surface layer, based on our previous findings, and was applied using the electrochemical deposition method. The substrate utilized was an open-porosity zinc foam fabricated via the investment casting technique. The primary objective of this experiment was to determine the optimal conditions for the deposition of the ceramic layer, aiming to achieve uniform, homogeneous coatings with suitable morphology and strong adhesion to the substrate.

Materials and methods

As cast open-cell zinc foams with 13 pores per inch pore density were used as a substrate. All the samples were ultasonically cleaned in ethanol (96 vol%) prior to the experimentes, dried at 50 °C for 1 hour and weighted. Electrochemical deposition of the hydroxyapatite (HAp) was carried out using an Autolab M204 multi channel potentiostat. Zn foam was used as the working electrode, arcgentochloride electrode (Ag/AgCl/KCl (3 mol/l)) as the reference electrode and Pt sheet as the counter electrode. HAp was deposited from the electrolyte consisting of 2.5 × 10-2 mol/l $NH_4H_2PO_4$ and 4.2 × 10-2 mol/l $Ca(NO_3)_2$. The solution composition was chosen according to the previous experimental procedures used for HAp electrochemical deposition onto metallic substrates such as iron (Fe) or titanium alloy (Ti_6Al_4V) [5]. Cathodic deposition was performed at three different conditions using various deposition time and current densities (Tab. 1). Scanning electron microscopy (SEM) with energy dispersive X-ray spectroscopy (EDS) analysis was performed to study the deposited coatings (Fig. 1).

Tab. 1: Comparison of different conditions for hydroxyapatite electrochemical deposition onto zinc foam substrate

	Time of deposition [min]	Current density [mA/cm^2]
Deposition Method 1	60	28
Deposition Method 2	30	56
Deposition Method 3	60	56

Results

Three types of coatings were prepared and analyzed under the conditions specified in Tab. 1. These conditions were selected based on prior findings obtained during the deposition of coatings on bulk substrates. In the case of Method 1, distinct ceramic coating islands were observed; however, these deposits did not achieve full surface coverage of the substrate (Fig. 1a). Method 3 yielded the least favorable results, as EDS analysis either failed to confirm or detected only minimal traces of the ceramic coating. Similar observations were made through SEM images (Fig. 1c). The most successful coating deposition was achieved under conditions of 30 minutes of electrodeposition at a current density of 56 mA/cm². The presence of the ceramic layer was confirmed by EDS analysis. SEM imaging (Fig. 1b) revealed that the deposited coating exhibited a relatively uniform morphology, characterized by a petal-like structure interspersed with rectangular crystals, which are likely associated with not only hydroxyapatite, but also calcium phosphate deposition. Further analyses are required to definitively determine the chemical composition of the deposited layer. Additionally, future investigations should explore the potential use of precursor treatments to enhance coating adhesion, as well as the incorporation of additives to suppress hydrogen gas evolution, which can induce cracking during the deposition process.

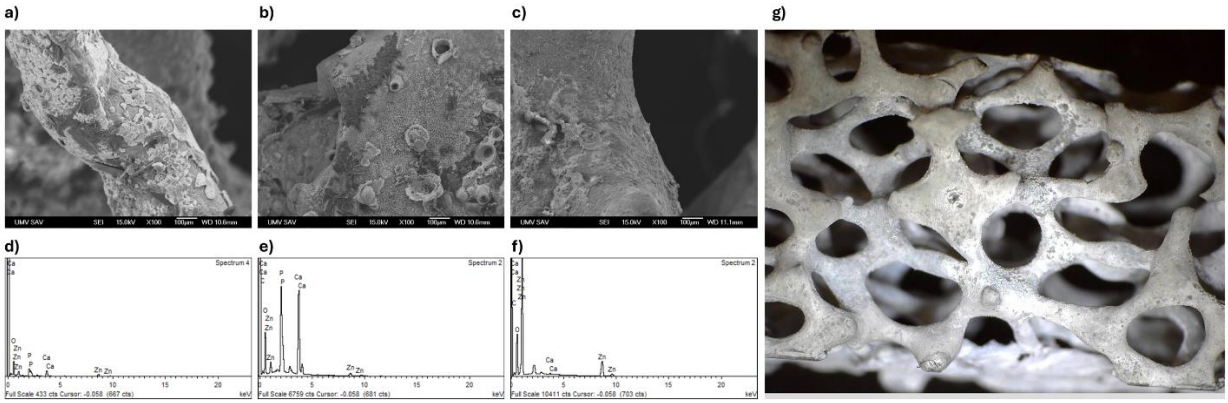

Fig. 1: SEM micrographs of the HAp coated zinc foams at 100× magnification prepared under different electrochemical conditions with corresponding EDS results: a,d) Deposition Method 1; b,e) Deposition Method 2; c,f) Deposition Method 3; g) Optical image of the representative HAp-coated zinc foam prepared under Deposition Method 2 conditions.

Acknowledgements

This work was funded by the EU NextGenerationEU through the Recovery and Resilience Plan for Slovakia under the project ZETA no. 09I03-03-V04-00010.

References

[1] Y. Liu, Y. Zheng, X.-H. Chen, J.-A. Yang, H. Pan, D. Chen, L. Wang, J. Zhang, D. Zhu, S. Wu, K. W. K. Yeung, R.-C. Zeng, Y. Han, S. Guan, "Fundamental theory of biodegradable metals—definition, criteria, and design" *Adv. Funct. Mater.*, vol. 29, no. 18, Feb. 2019, doi.org/10.1002/adfm.201805402.

[2] H. F. Li, Z. Z. Shi, L. N. Wang, " Opportunities and challenges of biodegradable Zn-based alloys" *JMST*, vol. 46, June 2020, doi.org/10.1016/j.jmst.2019.12.014.

[3] Y. Shi, Z. Xue, P. Li, S. Yang, D. Zhang, S. Zhou, Z. Guan, Y. Li, L.-N. Wang, "Surface modification on biodegradable zinc alloys" ACS Biomater. Sci. Eng., vol. 10, no. 9, p.p. 5454-5473, 2024, https://doi.org/10.1016/j.jmrt.2023.06.149.

[4] J. Rao, H. Gao, J. Sun, R. Yu, D. Zhao, Y. Ding, "A critical review of biodegradable zinc alloys toward clinical applications" Biomaterials Advances, vol. 136, 212792, 2022.

[5] R. Gorejová, R. Oriňaková, Z. O. Králová, T. Sopčák, I. Šišoláková, M. Schnitzer, M. Kohan, R. Hudák, "Electrochemical deposition of a hydroxyapatite layer onto the surface of porous additively manufactured Ti_6Al_4V scaffolds" *Surf. Coat. Tech.*, vol. 455, p.p. 129207, Feb. 2023, doi.org/10.1016/j.surfcoat.2022.129207.

Preparation of Glucose Sensor Based on TiO_2 Nanoparticles

J. Shepa[a]*, R. Filip[a], I. Shepa[b], N. Király[c], I. Šišoláková[a], R. Oriňaková[a]

[a] Department of Physical Chemistry, University of P. J. Šafárik in Košice, Moyzesova 11, 040 01 Košice, Slovak Republic

[b] Institute of Materials Research, Slovak Academy of Sciences, Watsonova 47, 040 01 Košice, Slovak Republic

[c] Department of Inorganic Chemistry, University of P. J. Šafárik in Košice, Moyzesova 11, 040 01 Košice, Slovak Republic

*jana.shepa@upjs.sk

Globally, the most prevalent causes of fatal body disorders such as cardiovascular and liver diseases include poor lifestyle and the associated prevalence of diabetes. A well-known procedure for the prevention and diagnosis of this disease is the continuous measurement of blood glucose levels affected patients. Despite well-established and accurate laboratory procedures, the scientific world is still looking for new, cheaper and more efficient ways to monitor glucose levels in blood [1]. Enzymatic sensors have gained leadership for many decades due to their unique properties, but their negative characteristics (low stability and high cost) have led scientists to investigate more stable, greener and cheaper equivalents - non-enzymatic sensors. Catalytically active substances that replace the function of enzymes without their high demands on the handling environment are the subject of many studies and open a wide range of new possibilities. The vision is to construct a non-invasive, environmentally friendly, inexpensive, and at the same time highly selective and stable sensor that will allow continuous sensing of patient´s glycemia [2].

Titanium and titanium dioxide have shown interesting properties in relation to glucose detection. The formation of a bond between the glucose molecule and the titanium dioxide nanotubes was observed and confirmed, forming a ligand-to-metal charge transfer complex compound [3]. Herein, preliminary results of titanium dioxide´s affinity to glucose are presented. However, for further measurements, a new approach was chosen - a screen-printed carbon electrode (SPCE) platform modified with rutile nanoparticles (TiO_2 NP) with dimensions less than 100 nm, which possess attractive properties, promising good reproducibility, high stability, low cost and reliability. The use of SPCE improves measurement efficiency, using a small sample volume (60 µL) and by miniaturizing the device, it facilitates handling. The aim of our current work is to focus on the optimization of the device preparation, the determination of the appropriate number of nanoparticles to modify the surface of the working electrode and the selection of a modification method with a sufficiently high degree of homogenization of the active surface.

Infrared and Raman spectroscopy were used to investigate the resulting complex of titanium and glucose nanoparticles. Three samples - glucose, TiO_2 NP + Nafion without immersion and TiO_2 NP + Nafion immersed in glucose solution for 24 hours - were subjected to infrared spectroscopy. The spectra were measured in the range 4000-400 cm^{-1}. Samples of glucose, TiO_2 NP + Nafion deposited on aluminium foil without contact with glucose solution and TiO_2 NP + Nafion deposited on aluminium foil and immersed for 24 hours in glucose solution were selected for analysis by Raman spectroscopy.

The Raman spectroscopy plots for different samples are shown in the Fig. 1. The typical active modes for rutile form of TiO_2 are A_{1g} (~610 cm^{-1}) + B_{1g} (~144 cm^{-1}) + B_{2g} (~826 cm^{-1}) + E_g (~445 cm^{-1}). Raman spectra for sample TiO_2 + Nafion (red curve) include all above-mentioned peaks, rest of peaks pertain to Nafion polymer film. Raman spectrum for glucose display low intensity of signal only two peaks are visible around 650 cm^{-1} and 700 cm^{-1}. Spectrum for TiO_2 + Nafion + glucose sample include wide variety of peaks. 144, 449, 610, and 826 cm^{-1} are signals typical for rutile; values of 671, 1127 and 1251 cm^{-1} can be assigned to the glucose molecule; 580, 729, 826, 976, 1435 cm^{-1} are signals originating from Nafion. The signals with values of 1578 and 1650 cm^{-1} do not belong to the Nafion, TiO_2 nanoparticles, or glucose molecule, and can therefore be assumed to belong to the bonds in the newly formed complex of TiO_2 and glucose.

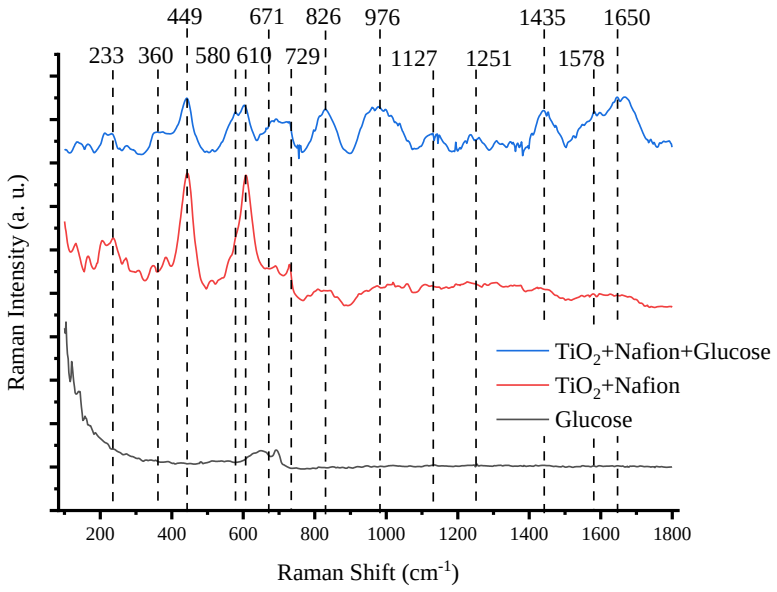

Fig. 1: Raman spectra of glucose (black line), TiO_2 + Nafion on aluminium foil (red line), TiO_2 + Nafion + glucose on aluminium foil (blue line).

The result of the infrared spectrum (Fig. 2) of TiO_2 NP + Nafion + glucose shows the following significant signals: 3220 cm^{-1}, which corresponds to the valence deformations of the hydroxyl groups in ν(OH); 2967 cm^{-1} apparently correspond to the symmetric and asymmetric vibrations in ν(CH_2) and ν(CH), respectively; 1737 cm^{-1} can be assigned to the valence vibration of the carbonyl group; 1365 cm^{-1} is located in the region of deformation vibrations of the δ(CH_2) and δ(CH) bonds; the signals with values of 916 and 851 cm^{-1} correspond to the region of valence vibrations ν(Ti-O).

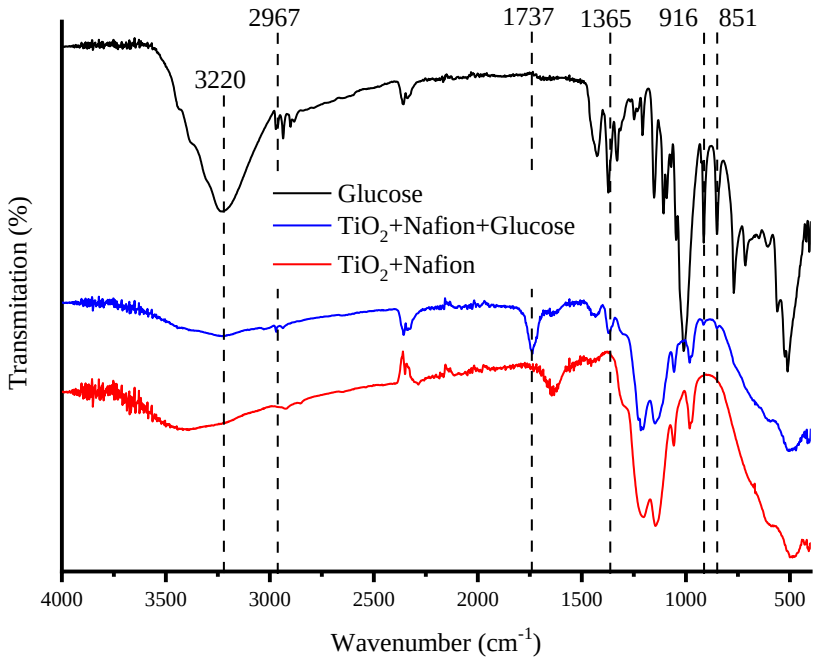

Fig. 2: Infrared spectra spectra of glucose (black line), TiO_2 + Nafion (red line), TiO_2 + Nafion + glucose (blue line).

Based on the above-mentioned results, the bond creation between the TiO_2 and glucose molecule was proven. Moreover, the presence of Nafion membrane used for the fixation of TiO_2 nanoparticles does not prevent interaction between both compounds. In conclusion, this platform is a suitable candidate for glucose sensor creation and miniaturization of the electrochemical system.

Acknowledgements

This work was funded by the EU NextGenerationEU through the Recovery and Resilience Plan for Slovakia under the project No. 09-I05-03-V02-00047.

References

[1] K. Singh, T. Agarwal, U. Kumar, S. Pal, A. Runthala, T.-M. Pan, C. C. Wu, “Optical biosensors for diabetes management: Advancing into stimuli-responsive sensing mechanisms”, *Smart Mater Med*, vol. 4, pp. 91–101, Jan. 2023, doi: 10.1016/j.smaim.2022.08.003.

[2] Q. Huang, J. Chen, Y. Zhao, J. Huang, and H. Liu, “Advancements in electrochemical glucose sensors”, Jan. 2025, *Elsevier B.V.* doi: 10.1016/j.talanta.2024.126897.

[3] J. Hovancová, I. Šišoláková, P. Vanýsek, R. Oriňaková, I. Shepa, M. Kaňuchová, N. Király, M. Vojtko, P. Čudek, A. Oriňák, "Ligand-to-metal charge transfer (LMCT) complex: New approach to non-enzymatic glucose sensors based on TiO_2", *Journal of Electroanalytical Chemistry*, vol. 878, Dec. 2020, doi: 10.1016/j.jelechem.2020.114589.

An In-Depth Study of the Mechanism Behind Hydrogen Evolution Reaction Catalyzed by Molybdenum Phosphide Across Diverse Media

N. Podrojková[a], A. Gubóová[b], M. Strečková[b], R. Oriňaková[a]*

[a] Institute of Chemistry, Faculty of Science, Pavol Jozef Safarik University in Košice, Moyzesova 11, 040 01 Kosice, Slovak Republic

[b] Institute of Materials Research, Slovak Academy of Sciences, Watsonova 47, 040 01 Kosice, Slovak Republic

*renata.orinakova@upjs.sk

Considering the influence of climatic conditions, the constraints associated with conventional resources, and the increasing energy demand, hydrogen production via electrolytic water splitting is a promising technological solution [1]. This method's efficacy lies in its ability to produce clean and renewable hydrogen, which is notable for its substantial storage capabilities, high energy density, and environmentally sustainable characteristics [2].

In electrochemical water splitting, two half-reactions are fundamental: the oxygen evolution reaction (OER) at the anode and the hydrogen evolution reaction (HER) at the cathode [3]. The HER process at the cathode depends on the electrolyte's pH, as evidenced by the equations presented below (eqs. 1-6) [4].

Acidic solution:

$$H^+ + e^- \rightarrow H^* \text{ (Volmer)} \quad (1)$$

$$H^+ + e^- + H^* \rightarrow H2 \text{ (Heyrovsky)} \quad (2)$$

$$\text{or } 2H^* \rightarrow H_2 \text{ (Tafel)} \quad (3)$$

Alkaline or neutral solution:

$$H_2O + e^- \rightarrow H^* + OH^- \text{ (Volmer)} \quad (4)$$

$$H_2O + e^- \rightarrow H_2 + OH^- \text{ (Heyrovsky)} \quad (5)$$

$$\text{or } 2H^* \rightarrow H_2 \text{ (Tafel)} \quad (6)$$

The hydrogen evolution reaction (HER) is characterized by a two-step mechanism, wherein the adsorbed hydrogen atom (Hads) plays a crucial role as an intermediate that influences the overall reaction pathways. The first step, termed the Volmer reaction, involves the transfer of an electron to the electrode surface, which facilitates the reduction of a proton to generate H* in acidic solutions ($H^+ + e^- \rightarrow H^*$). In neutral or alkaline solutions, where protons are present

in very low concentrations, H* is formed by reducing water molecules with the transferred electron ($H_2O + e^- \rightarrow H^* + OH^-$). The second step of the hydrogen evolution reaction (HER) involves the production of gaseous hydrogen, which can occur via the Heyrovsky or Tafel pathways, depending on the specific coverage ratio of H* [4].

The electrolytic hydrogen evolution reaction (HER) faces considerable challenges, including the prohibitive costs of catalysts, the slow kinetics of the reaction, and its limited efficiency in terms of current densities [5]. As a result, there is an ongoing search for alternatives to platinum-group or platinum-based materials, which are acknowledged as the most effective electrocatalysts for HER [2].

Transition metal phosphides (TMPs) are considered to be highly efficient electrocatalysts for the hydrogen evolution reaction (HER), primarily due to their structural similarities to platinum-based catalysts. TMPs exhibit both covalent bonding between metal (M) and phosphorus (P) and metallic bonding (M–M). The covalent bonds enable charge storage through Faradaic redox processes, which enhances their capacity. In contrast, the metallic bonds facilitate the flow of free electrons, thereby improving electrical conductivity and expediting charge transfer. Furthermore, the high electronegativity of phosphorus leads to the formation of negatively charged P atoms and positively charged metal atoms, which act as centers for proton and hydride acceptance. This synergistic interaction fosters an enhanced efficiency in the HER [6].

Molybdenum phosphide (MoP) demonstrates outstanding catalytic performance for the hydrogen evolution reaction (HER), coupled with high thermal stability and cost-effectiveness. These attributes have garnered considerable research interest, positioning MoP as a promising alternative to platinum-group catalysts [2]. MoP's electrocatalytic properties are particularly noteworthy, as its electronic structure closely resembles that of platinum-group catalysts. It also exhibits exceptional stability and effective performance across a broad pH range [7].

An in-depth understanding of the molybdenum phosphide (MoP) catalytic mechanism is crucial for developing superior hydrogen evolution reaction (HER) catalysts. The application of density functional theory (DFT) can significantly enhance the insight into the relationship between HER activity and the various facets of MoP. Zhang et al. were among the first researchers to apply DFT to examine HER on the MoP(001) surface [8]. Their research revealed that HER can occur on both P- and Mo-terminated surfaces in acidic conditions through different pathways. In neutral environments, HER may occur on P-terminated surfaces, especially when surface defects are present. Gao et al. explored the HER on six distinct MoP2 facets, including (111), (110), (101), (001), and (01$\bar{1}$), employing spin-polarized DFT [9]. The results demonstrated that MoP2(111) possesses commendable activity for the hydrogen evolution reaction (HER) across a diverse range of hydrogen coverages. The catalytic activity for HER in MoP2(111) can be enhanced by doping the phosphorus sites with nitrogen or sulfur atoms and substituting iron atoms at the molybdenum sites. Gao et al. also utilized density functional theory (DFT) to support their experimental results [10]. Their DFT studies revealed that the interaction of the MoP(111) surface with hydrogen is primarily mediated by the phosphorus sites, which are responsible for hydrogen adsorption and act as conduits for hydrogen atom delivery, thus facilitating HER.

The literature on the various facets of molybdenum phosphide (MoP) and their comparative behavior in environments with differing pH levels is notably limited. In their study, Dong et al. employed density functional theory (DFT) to

investigate the MoP facets, specifically (001), (010), (100), (011), (110), and (111), as well as the Co/C doped MoP(111) facet, to gain insights into the hydrogen evolution reaction (HER) in acidic conditions [19]. Their findings indicate that judicious doping with heteroatoms can enhance the HER activity of MoP catalysts significantly; however, excessive doping may result in electron reflux, which can increase adsorption and reduce hydrogen production.

Therefore, in this research, we examine the impact of different environmental conditions—acidic (0.5 M H_2SO_4), alkaline (1 M KOH), and neutral (1 M PBS)—on the electrocatalytic performance of hydrogen production from molybdenum phosphide (MoP) surfaces featuring various facets, namely MoP(101), MoP(110), and MoP(100), through density functional theory (DFT) calculations. The results obtained from computational analyses were compared with the electrochemical performance of the hydrogen evolution reaction (HER) in the environments mentioned above. For a comprehensive understanding, the experimental protocols and characterization techniques were included. This investigation integrates theoretical simulations of MoP surfaces with experimental assessments of MoP as an electrocatalyst, aiming to deepen the understanding of the HER mechanism. The findings not only contribute to the fundamental understanding of the HER mechanism but also have practical implications for the development of transition metal phosphide (TMP) electrocatalysts and their potential future applications in electrolysers and fuel cells.

Acknowledgements

This work was funded by the EU NextGenerationEU through the Recovery and Resilience Plan for Slovakia under the project No. 09I03-03-V04-00086.

References

[1] T. Liu, X. Zhao, X. Liu, W. Xiao, Z. Luo, W. Wang, Y. Zhang, J.C. Liu, “Understanding the hydrogen evolution reaction activity of doped single-atom catalysts on two-dimensional GaPS4 by DFT and machine learning,” J. Energy Chem. vol. 1, pp. 93–100, 2023, doi: 10.1016/j.jechem.2023.02.018.

[2] O. O. Dada, S. Karimzadeh, P.E. Imoisili, T.C. Jen, “Theoretical insights of electrocatalytic hydrogen evolution on MoP nanocrystal,” Int. J. Hydrogen Energy. vol. 48, pp. 34634–34648, 2023, doi: 10.1016/j.ijhydene.2023.05.302.

[3] Z. Li, L. Sun, Y. Zhang, Y. Han, W. Zhuang, L. Tian, W. Tan, “Coupled and decoupled electrochemical water splitting for boosting hydrogen evolution: A review and perspective,” Coord. Chem. Rev. vol. 510, 215837, 2024, doi: 10.1016/j.ccr.2024.215837.

[4] A. Raveendran, M. Chandran, R. Dhanusuraman, “A comprehensive review on the electrochemical parameters and recent material development of electrochemical water splitting electrocatalysts,” *RSC Adv*., vol. 13, pp. 3843–3876, 2023, doi: 10.1039/d2ra07642j.

[5] M. S. S. Danish, “Exploring metal oxides for the hydrogen evolution reaction (HER) in the field of nanotechnology,” *RSC Sustain*., vol. 1, pp. 2180–2196, 2023, doi: 10.1039/d3su00179b.

[6] K. Bhunia, M. Chandra, S. Kumar Sharma, D. Pradhan, S.J. Kim, "A critical review on transition metal phosphide based catalyst for electrochemical hydrogen evolution reaction: Gibbs free energy, composition, stability, and true identity of active site," *Coord. Chem. Rev*., vol. 478, 214956, 2023, doi: 10.1016/j.ccr.2022.214956.

[7] A. Guboova, R. Orinakova, M. Streckova, N. Podrojkova, M. Parackova, O. Milkovic, L. Medvecky, V. Girman, T. Bystron, "Bimetallic MoFe phosphide catalysts for the hydrogen evolution reaction," *Electrochim. Acta*., vol. 506, 145008, 2024, doi: 10.1016/j.electacta.2024.145008.

[8] Y. Zhang, H. Lei, D. Duan, E. Villota, C. Liu, R. Ruan, "New Insight into the Mechanism of the Hydrogen Evolution Reaction on MoP(001) from First Principles," *ACS Appl. Mater. Interfaces*., vol. 10, pp. 20429–20439, 2018, doi: 10.1021/acsami.8b03976.

[9] Y. Gao, H. Li, J. Wang, J. Ma, H. Ren, "New insight on hydrogen evolution reaction activity of MoP2 from a theoretical perspective," *Nanomaterials*., vol. 9, pp. 1–13, 2019, doi: 10.3390/nano9091270.

[10] Y. Gao, Q. Wang, T. He, J.Y. Zhang, H. Sun, B. Zhao, B.Y. Xia, Y. Yan, Y. Chen, "Defective crystalline molybdenum phosphides as bifunctional catalysts for hydrogen evolution and hydrazine oxidation reactions during water splitting," *Inorg. Chem. Front.*, vol. 6, pp. 2686–2695, 2019, doi: 10.1039/c9qi01005j.

Screen-printed Electrode Modified by Carbon Powder for Uric Acid Detection

V. Niščáková[a*], N. Jašňáková[a], J. Shepa[a], I. Šišoláková[a], R. Oriňaková[a]

[a]Department of Physical Chemistry, University of P. J. Šafárik in Košice, Moyzesova 11, 040 01 Košice, Slovak Republic

[*]veronika.niscakova@upjs.sk

One of the significant substances found in body fluids is uric acid (UA) produced by metabolic processes. Abnormal UA levels can cause kidney problems, such as hyperuricemia, Lesch-Nyhan syndrome, celiac disease, and gastrointestinal disorders. The preservation of human health and the early identification of diseases depend on the levels of relevant biomolecules being monitored. Many techniques, such as chemiluminescence, capillary electrophoresis, high-performance liquid chromatography, and spectroscopic methods, have been developed for UA detection [1]. These conventional techniques are costly, time-consuming, and need expert operation. On the other hand, electrochemical (EC) methods provide sensitive, quick, and affordable in situ monitoring, which makes them very appealing for applications involving simultaneous detection. Recent developments in optical and EC sensors have shown promising results by promoting redox reactions for quantitative analysis. EC sensors in particular allow for the continuous and accurate monitoring of brain biomarkers. However, the coexistence of AA, DA, and UA in biological fluids as well as the existence of interfering substances make simultaneous detection of these substances challenging [2].

Since carbon materials display a large specific surface area, high electrical conductivity, a wide electrochemical window for the electrochemical detection of different analytes, and a low cost, they are already well established and used in working electrodes (WE) modifications. Graphite is commonly used to process screen-printed WE because it is a special and significant material for the electrochemical detection of organic compounds [3].

Here, the graphite powder was used for screen-printed carbon electrode (SPCEs, Metrohm DropSens 11L) modification to enlarge an active surface area and enhance the electrochemical properties. The SPCE were modified by drop-casting method (1 µl) from solution including dispersed carbon powder (0.05 g) in ethanol : water (1:1) solution. All electrochemical measurements were carried out within a potential window from -1 to 1 V, a scan rate of 100 mV/s. These measurements were performed using a Solartron Analytical ModuLab Xm equipped with a connector for the SPCE system. All experiments were carried out at atmospheric pressure and laboratory temperature. For active surface area measurement, a 60 µl of 5 mM solution of $K_3[Fe(CN)_6]/K_4[Fe(CN)_6]$ in 1 M KCl was used.

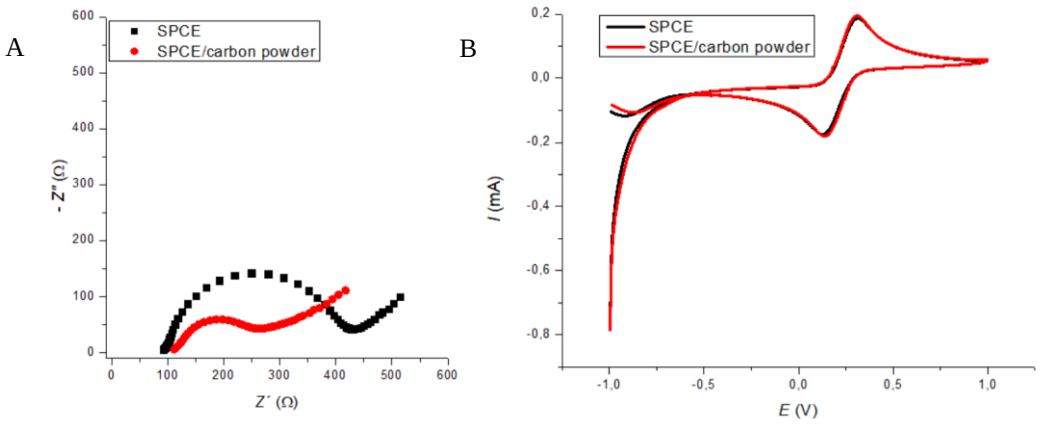

Fig. 1: Nyquist diagrams for SPCE and SPCE/graphite powder at OCP in 5 mM $K_3[Fe(CN)_6]/K_4[Fe(CN)_6]$ in 1 M KCl (A). Cyclic voltammograms for for SPCE and SPCE/graphite powder at OCP in 5 mM $K_3[Fe(CN)_6]/K_4[Fe(CN)_6]$ in 1 M KCl (B).

Electrochemical impedance spectroscopy was used for the phase interface properties. As shown on the Fig. 1, the Nyquist diagrams displays shape for typical Randles circuit. The charge transfer resistance of SPCE electrode was approx. 300 Ω and after the modification by graphite powder, the charge transfer resistance decrease to approx. 150 Ω. This behaviour indicated the enhancement of electron transfer through to phase interface. Active surface area was calculated by using Randles- Ševčík equation. The value of active surface area for SCPE electrode was 2.3 mm^2 and after the modifications of SPCE by graphite powder, the active surface area increased to 2.4 mm^2. I could be conclude that the electroactive surface area is without changes.

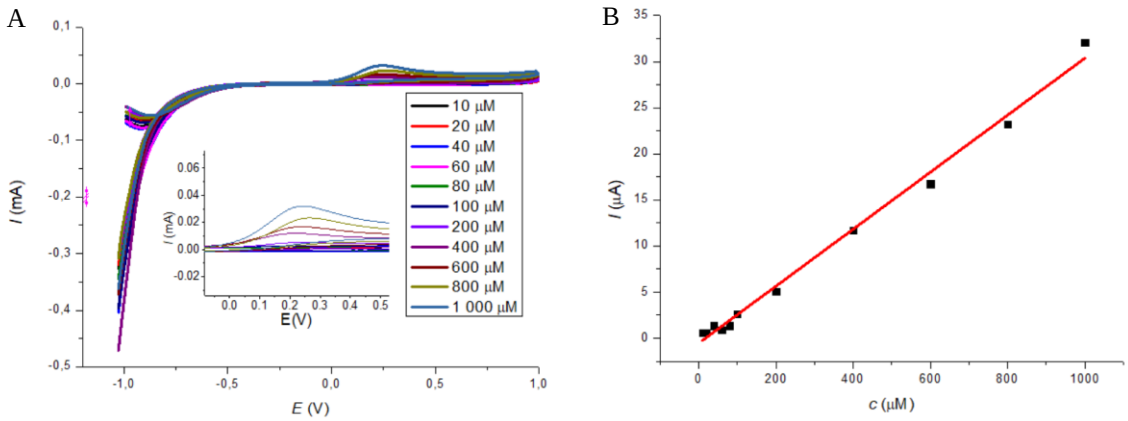

Fig. 2: Cyclic voltammograms for different concentrations of UA in PBS (10, 20, 40, 60, 80, 100, 200, 400, 600, 800, and 1000 µM) (A). Calibration curve for SPCE/graphite electrode (B).

The modified electrode was used for UA determination in PBS, which was used for simulation of body fluids, mainly in the case of Cl^- presence. Cyclic voltammogram for UA display 1 well defined oxidation peak at the potential 0.25 V without reduction peak presence. It indicates that the electrochemical oxidation of UA is irreversible process, which is expected behaviour for organic compound. For electrochemical measurement was used 60 µl of UA diluted in the PBS within the concentration range from 10 to 1000 µM. The sensitivity of modified electrode was 30.93 nA/µM and limit of detection 36.27 µM. The normal UA concentration in the blood is from 150 µM to 430 µM, so modified sensor covers whole range. So proposed sensor is promising candidate for UA detection in blood serum.

Acknowledgements

This work was funded by the EU NextGenerationEU through the Recovery and Resilience Plan for Slovakia under the project No. 09-I05-03-V02-00047.

References

[1] A. U. Rehman, M. Anwar, A. Khan, K. A. Kalhoro, C. Zhang, Y. Zhang, M. Shokouhimehr, Z. Liu, "Perforated MoS2 nanosheets adorned with Ni nanoparticles: An electrochemical sensor for concurrent detection of dopamine and uric acid," *Microchemical Journal*, vol. 209, Feb. 2025, doi: 10.1016/j.microc.2025.112821.

[2] L. Wang, J. Guo, G. M. Qian, Y. C. Li, L. Yu, and B. H. Xiao, "Electrochemical nanoprobe for highly sensitive and simultaneous detection of ascorbic acid, dopamine, and uric acid," *Microchemical Journal*, vol. 210, Mar. 2025, doi: 10.1016/j.microc.2025.112957.

[3] B. Repič, K. Radan, G. Marolt, A. B. Golob, and D. Kuscer, "Effect of processing temperature on performance of screen-printed graphite electrodes," *Mater Chem Phys*, p. 130455, Jan. 2025, doi: 10.1016/j.matchemphys.2025.130455.

Surface Treatment of Metallic Nickel Electrodes for Glucose Sensing

F. Märzweiler[a*], G. Fafilek[a]

[a] Research Group for Electrochemical Methods and Corrosion, TU Wien, Getreidemarkt 9/E164
* florian.maerzweiler@tuwien.ac.at

Disclosure

Due to upcoming patent proposals for the surface treatment of nickel and the resulting nickel biosensor, detailed information about the reaction mechanism, treatment procedure and results will not be disclosed.

Introduction

Modern biosensors for the measurement of the glucose level in blood rely on the enzymatic immobilization and oxidation of glucose using glucose oxidase and a redox mediator. An electrochemical signal is generated by oxidation of said redox mediator [1]. However, the application of glucose oxidase makes these biosensors subsceptible to environments unfavorable for the enzyme such as pH value and temperature [2].

Noble metals such as gold or platinum constitute attractive alternatives for glucose oxidase, allowing for direct oxidation of glucose in enzyme-free biosensors. However, chloride, which is ubiquitous in bodily fluids, affects the performance of those metals negatively by either acting as catalyst poison through coordinative bonding or reducing the number of active sites by chemisorption [3].

In our work, we present surface treated nickel as an alternative electrode material for glucose biosensors that is unaffected by the negative effects of chloride for measurements carried out below the pitting corrosion potential.

Results

Fig. 1 depicts the current measured at the glucose reaction potential with a surface treated nickel electrode, tested in solutions of glucose in PBS with concentrations of 5, 10, 20 and 40 mM. The value of 0 mM was recorded in PBS itself. The current is given in the total amount, without any specification to a positive or negative sign.

A linear correlation between the measured current and glucose concentration was observed, with a promising correlation coefficient of 0.9985.

In Fig. 2, the influence of the surface treatment on the measured current in a 40 mM solution of glucose in PBS is displayed. The figure shows that an untreated surface yields a current comparable to the absence of glucose at the treated electrode in Fig. 1, which is below 3 πA. However, with increasing degree of surface modification by the treatment, the current at the glucose reaction potential increases. This suggests that the treated surface enables the measurement of glucose and can enhance sensitivity.

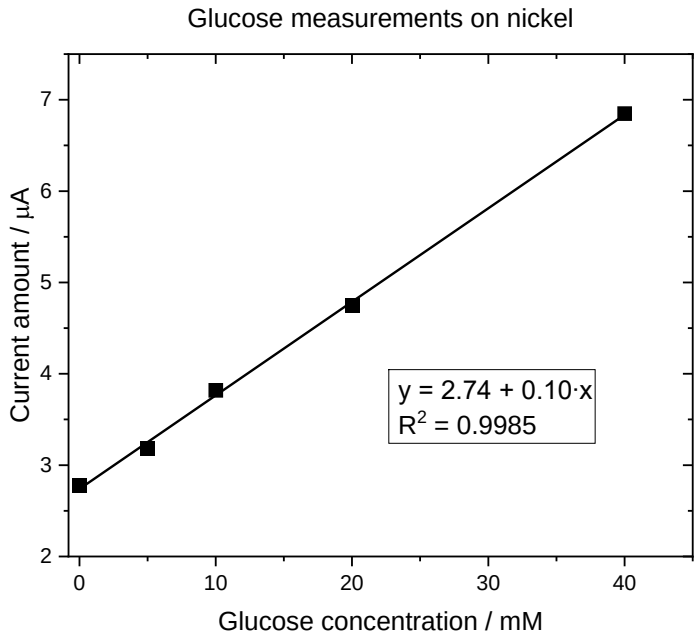

Fig. 1: Current measured with a treated nickel electrode for different glucose concentrations in PBS

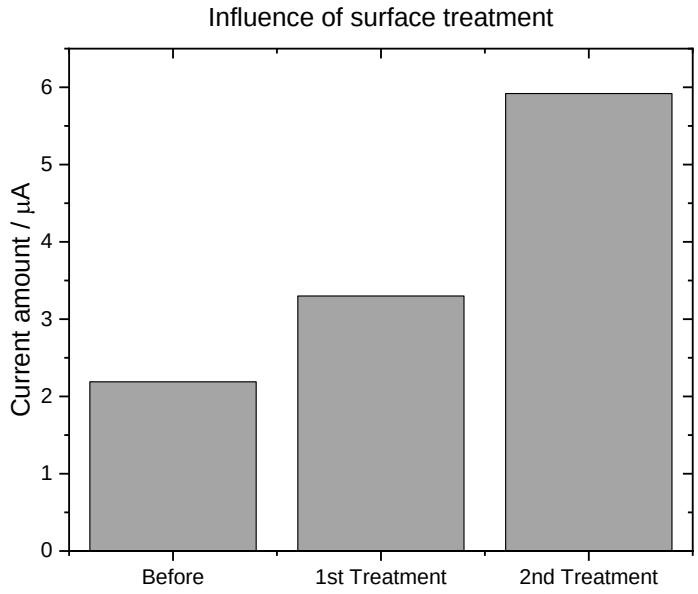

Fig. 2: Influence of surface treatment on the current measured in a 40 mM solution of glucose in PBS

Summary

The results show that surface treated nickel is a viable alternative for the non-enyzmatic detection of glucose. Furthermore, glucose could be quantified in the concentration range of 5 to 40 mM, showing a linear correlation between the measured current and glucose concentration. Therefore, a biosensor employing nickel is potentially applicable for blood sugar measurements in human blood, as human glucose levels are normally between 4 to 6 mM [4].

Outlook

In future experiments, the modified nickel surface will be investigated using electrochemical impedance spectroscopy (EIS) to quantify the surface capacitance. Furthermore, an in-situ XRD cell [5] will be utilized to monitor and confirm the mechanism of the surface treatment.

As the measuring principle of the nickel biosensor is also applicable to other organic molecules of suitable chemical structure, the linear detection range as well as the detection limit of the sensor will be tested for different relevant analytes, such as environmentally harmful compounds.

Acknowledgements

This research was sponsored by the NATO Science for Peace and Security Programme under grant id. G6106

References

[1] M. Wei, Y. Qiao, H. Zhao, J. Liang, T. Li, Y. Luo, S. Lu, X. Shi, W. Lu, X. Sun, “Electrochemical non-enzymatic glucose sensors: recent progress and perspectives”, *Chem. Commun*, vol. 56, pp. 14553-14569, Sep. 2020, doi: 10.1039/d0cc05650b.

[2] J. Wang, “Electrochemical Glucose Biosensors”, *Chem. Rev.*, vol. 108, pp. 814-825, Dec. 2008, doi: 10.1021/cr068123.

[3] X. Xu, A. Makaraviciute, J. Petterson, S.-L. Zhang, L. Nyholm, Z. Zhang, “”Revisiting the factors influencing gold electrodes prepared using cycling voltammetry”, *Sens. Actuators B Chem.*, vol. 283, pp. 146-153, Dec. 2018, doi:10.1016/j.snb.2018.12.008.

[4] A. W. Norman, H. L. Henry, “Hormones”, 3rd ed. Cambridge, Cam, *USA: Academic Press Inc*., 2015

[5] F. Froech, S. Kubicek, W. Artner, M. Nelhiebel, S. Larisegger, G. Fafilek, “A versatile electrochemical cell for *in-situ* GI-XRD measuremetns on lab-scale XRD devices”, *J. Electroanal. Chem.*, vol. 971, pp. 118591-118596, Aug. 2024, doi: doi.org/10.1016/j.jelechem.2024.118591.

Functionalized Citrate-Based Polyesters with Bioactive Compounds for Tissue Engineering

T. Sopcak[a]*, L. Medvecky[a], T. Csanádi[a], M. Dzupon[a], M. Giretova[a], R. Stulajterova[a], F. Kromka[a], O. Petrus[a], M. Faberova[a], P. Jevinova[b]

[a]Institute of Materials Research of SAS, Watsonova 47, 04001 Kosice, Slovak Republic

[b]Department of Food Hygiene, Technology and Safety, University of Veterinary Medicine and Pharmacy, Komenského 73, 041 81 Košice, Slovakia

*tsopcak@saske.sk

Polymeric biomaterials are important materials in biomedicine that can provide tailored properties to meet the requirements of tissue engineering, drug delivery and bioimaging applications. Among them, biodegradable polyesters are particularly encouraging due to their tunable mechanical properties, controlled degradation and excellent biocompatibility, making them suitable for biomedical applications [1]. Over a broad range of polyesters, including polylactides and lactones, there has been growing interest in newer varieties in recent years. For instance, polyol-based polyesters, which are synthesized through the polycondensation of multifunctional carboxylic acids, such as citric acid, with polyhydric alcohols of varying chain lengths, result in biopolyesters that offer a broader range of physicochemical and biological properties compared to traditional polylactides [2]. Typical polyol citrates include poly(1,4-butanediol citrate; PBC), poly(1,8-octanediol citrate; POC), poly(1,10-decanediol citrate; PDC), and glycerol citrate (GCA), with the majority of research to date, however, focused on POC-based citrate [2]. Although polyol citrates have shown great potential in both soft and hard tissue engineering, none of the above are currently used in their pure, unmodified form due to inadequate biodegradation, limited bioactivity, and a narrow range of mechanical properties. Therefore, further functionalization is necessary to enhance their performance and broaden their applicability in biomedical fields [3].

POC polyesters have been extensively functionalized with a wide range of bioactive and non-bioactive compounds, including both organic and inorganic components (Fig. 1). These modifications involve carboxylic acids, diols, urethanes, glutathione, expanded polytetrafluoroethylene, amino acids, as well as inorganic materials such as silica, zinc oxide, graphene, bioactive glasses, and calcium phosphates [2]. In contrast, the functionalization of GCA polyesters has been far less explored, primarily focusing on composite materials with bioactive calcium phosphates [4,5]. Given the limited research on GCA polyesters, further investigation into their modification strategies is valuable, particularly to enhance biocompatibility, extend biodegradation time, and improve mechanical properties.

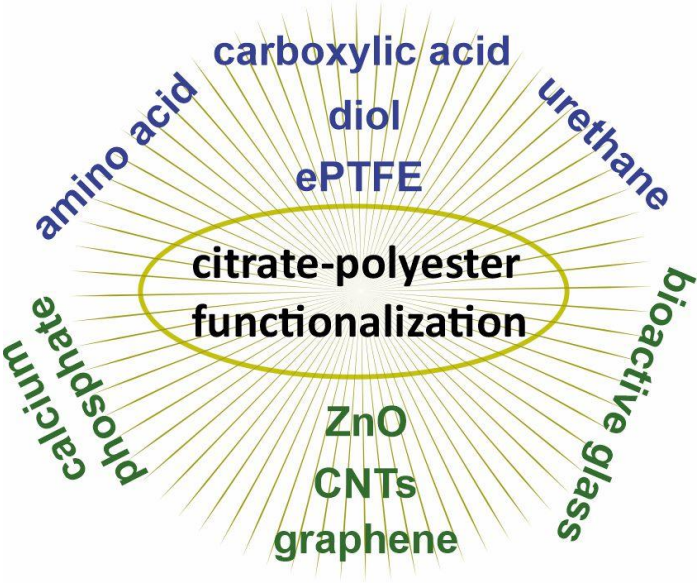

Fig. 1: Functionalization of citrate polyesters with various compounds

In recent years, natural bioactive compounds with a phenolic core, present in many plant extracts, have gained increasing attention due to their diverse biological activities, such as antimicrobial, antioxidant, anti-inflammatory, and antifungal properties [6]. Among them, polyphenols like tannic acid (TA) offer significant advantages over simple phenolic compounds as a result of their enhanced hydrophilicity, lower volatility, improved degradability, and greater ability to be incorporated into polymeric backbones. The unique chemical structure of TA, consisting of multiple hydroxyl (OH) groups, enables strong interactions with various polymeric networks, allowing their properties to be tailored [7]. TA, as a versatile crosslinking agent and modifier, may offer promising opportunities for functionalizing polyesters, including citrate-based polymers, to enhance their multifunctional physicochemical and biological properties for biomedical applications. The main functionalizations and properties of modified citrate polyesters will be summarized, with particular emphasis on our recent contributions toward their development for tissue engineering applications.

Acknowledgements

This work was funded by the EU NextGenerationEU through the Recovery and Resilience Plan for Slovakia under the project No. 09I03-03-V04-00133.

References

[1] H. Ye, K. Zhang, D. Kai, Z. Li, X.J. Loh, "Polyester elastomers for soft tissue engineering," *Chem. Soc. Rev.*, vol. 47, no. 12, pp. 4545–4580, May 2018, doi.org/10.1039/C8CS00161H.

[2] M. Wang, P. Xu, B. Lei, "Engineering multifunctional bioactive citrate-based biomaterials for tissue engineering," *Bioact. Mater*., vol. 19, pp. 511-537, January 2023, doi.org/10.1016/j.bioactmat.2022.04.027.

[3] Y. Du, J. Ge, Y. Shao, P.X. Ma, X. Chen, B. Lei, "Development of silica grafted poly(1,8-octanediolco- citrates) hybrid elastomers with highly tunable mechanical properties and biocompatibility," *J. Mater. Chem. B.*, vol. 3, no. 15, pp. 2986-3000, February 2015, doi.org/10.1039/C4TB02089H.

[4] T. Sopcak, L. Medvecky, M. Giretova, R. Stulajterova, J. Brus, M. Urbanova, F. Kromka, M. Podobova, M. Faberova, "Fabrication of a glycerol-citrate polymer coated tricalcium phosphate bone cements: Structural investigation and material properties," *J. Polym. Res.*, vol. 28, no. 231, June 2021, doi.org/10.1007/s10965-021-02596-w.

[5] Y.Q. Shen, Y.J. Zhu, H.P. Yu, B. Qiang, "Biodegradable nanocomposite of glycerol citrate polyester and ultralong hydroxyapatite nanowires with improved mechanical properties and low acidity," *J. Colloid. Interf. Sci.*, vol. 530, pp. 9-15, June 201, doi.org/10.1016/j.jcis.2018.06.059.

[6] S. Martins, S.I. Mussatto, G. M. Avila, J. M. Saenz, C. N. Aguilar, J. A. Teixeira, "Bioactive phenolic compounds: Production and extraction by solid-state fermentation. A review," *Biotechnol. Adv*. Vol. 23, no. 3, pp. 365-373, June 2011, doi.org/10.1016/j.biotechadv.2011.01.008.

[7] C. Chen, H. Yang, X. Yang, Q. Ma, "Tannic acid: a crosslinker leading to versatile functional polymeric networks: a review," *RSC Adv*., vol. 12, no. 13, pp. 7689–7711, March 2022, doi.org/10.1039/D1RA07657D.

Efficient Transition Metal Electrocatalysts for Water Splitting

M. Strečková[a]*, A. Guboová[a], N. Podrojková[b], R. Oriňáková[b]

[a]Institute of Materials Research, Slovak Academy of Sciences, Watsonova 47, 040 01 Kosice, Slovak Republic

[b]Institute of Chemistry, Faculty of Science, P.J. Safarik University, Moyzesova 11, 040 01 Kosice, Slovak Republic

*mstreckova@saske.sk

The global demand for energy is undergoing significant transformation. Hydrogen is emerging as the energy carrier of the future and is expected to play a key role in developing a more sustainable industry and society. However, hydrogen is currently produced mainly from fossil fuels, which makes it unsuitable for decarbonization efforts. As a result, water electrolysis appears to be a promising alternative. Alkaline water electrolysis (AWE) and Polymer Electrolyte Membrane (PEM) water electrolysis, with advanced technologies, offer the greatest potential for this transition, enabling the large-scale production of green hydrogen using renewable energy sources.

The production of industrial electrolyzers often involves platinum-based elements, which makes them less competitive for large-scale hydrogen production. Identifying effective alternatives is crucial for making water electrolysis a viable technology for hydrogen production. Both AWE and PEM electrolyzers operate on the same basic principle: two half-cells, consisting of an anode and cathode, where the oxygen evolution reaction (OER) and hydrogen evolution reaction (HER) take place. Among these two reactions, the OER is more challenging both thermodynamically and kinetically. In addition to having access to renewable electricity for the OER, developing durable and abundant electrocatalysts for both the OER and HER remains a significant challenge for large-scale water electrolysis.

Among various physicochemical properties, the electrocatalyst surface and its interaction with water, reaction intermediates, and the formed hydrogen and oxygen molecules are crucial to catalytic performance and the reaction mechanism. Specifically, the binding strengths between the catalyst surface and intermediates determine the rate-limiting step and electrocatalytic performance.

This account provides insights into the hydrogen economy's status and the basic principles of water electrolysis, covering both its fundamentals and industrial advancements. Additionally, the reaction mechanisms of HER and OER in water electrolysis and recent progress in electrocatalysts for both half-reactions are discussed. The study also explains the effects of different morphologies and structures of molybdenum-based electrocatalysts, with specific references. A particular focus is placed on the enhancement of intrinsic activity through density functional theory (DFT) calculations. The structural modification and phase transformation of transition metal phosphide electrocatalysts under three-electrode setups are also examined. Furthermore, the activation of cobalt- and nickel-based electrocatalysts through iron uptake from the alkaline electrolyte is discussed. This study provides a brief overview of the challenges related to the large-scale production and utilization of green hydrogen.

Acknowledgements

This work was financially funded by the EU NextGenerationEU through the Recovery and Resilience Plan for Slovakia under the project No. 09I03-03-V04-00109.

Study of the Processes Taking Place During the Electrochemical Detection of SARS-CoV-2 Spike Protein

N. Jašňáková[a]*, J. Shepa[a], I. Šišoláková[a], R. Oriňaková[a]

[a] Department of Physical Chemistry, Faculty of Science, Pavol Jozef Šafárik University, Moyzesová 11, 04011 Košice, Slovak Republic

*nikola.jasnakova@student.upjs.sk

Introduction

Electrochemical detection techniques have a pivotal role in precise virus identification and the prevention of pathogen transmission, particularly during global health crises such as the COVID-19 pandemic. The performance of modern electrochemical sensors is significantly enhanced through the integration of nanomaterials and biomolecules, among which streptavidin is widely utilized due to its strong affinity to biotin. The specific interaction is used in aptasensors to facilitate efficient charge transfer processes [1, 2, 3].

This study presents the development of an advanced electrochemical biosensor for SARS-CoV-2 detection, employing an aptamer immobilized on screen-printed carbon electrodes (SPCE) functionalized with streptavidin-modified surfaces. The Nicholson equation [4] is applied to investigate the electron transfer kinetics within the system, providing a comprehensive understanding of charge transfer mechanisms in electrochemical biosensor. A combination of experimental measurements and theoretical equations enables the determination of key dynamic parameters governing reaction kinetics. These findings contribute to the advancement of electrochemical detection methodologies.

Experimental conditions

Screen-printed carbon electrodes (SPCEs) from Metrohm, Switzerland, were pre-modified with streptavidin to facilitate specific binding with biotinylated aptamer. For aptamer immobilization was applied 10 µL of the aptamer solution (Apt CoV2-RBD-4C 5AA) to the working electrode followed by incubation at 5 °C for 1 hour. After incubation, excess liquid was removed using compressed air. Subsequently, 10 µL of spike protein was added to the aptamer-modified electrode and incubated for 30 minutes at 5 °C. Then the excess liquid was removed using compressed air. Electrochemical measurements were performed using the potentiostat Solartron Analytical Modulab (Model 2100 A, CA) and 60 µL of a 5 mM solution of $K_3[Fe(CN)_6]/K_4[Fe(CN)_6]$ in 1M KCl.

Discussion

Mechanism and kinetic parameters of electrochemical reaction were studied via cyclic voltammetry method. Cyclic voltammograms for different electrode modifications at various scan rates are shown on the Fig. 1. For all

modifications the peak current increase with the scan rate and the oxidation and reduction peak shifted away from each other. Moreover, the peak separation was more than 50 mV, it could be expected that the electrochemical system is quasi-reversible.

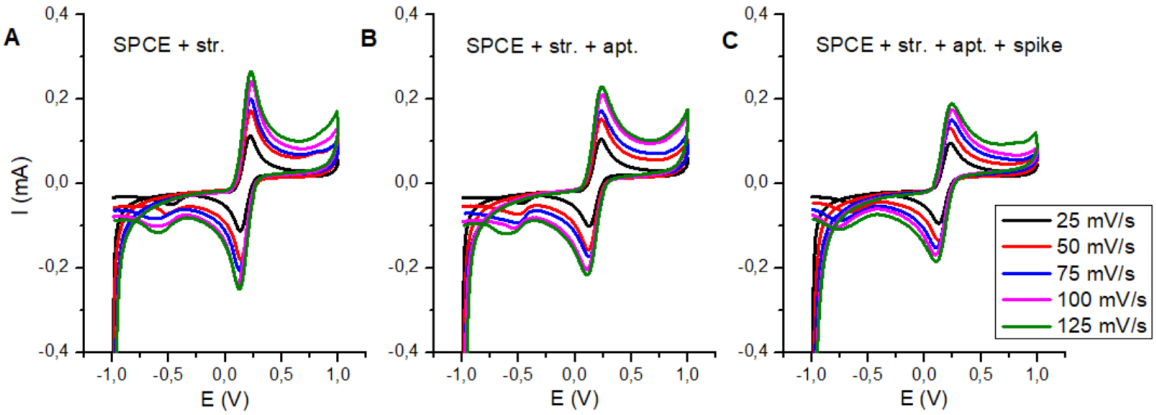

Fig. 1: Cyclic voltammograms for different modification of SPCE electrode (SPCE + str. (A), SPCE + str. + apt. (B), and SPCE + str. + apt. + spike (C)) at various scan rates (25, 50, 75, 100, and 125 mV/s).

Linear dependences of log *I* on log *v* for different modification of SPCE electrodes were fitted by linear function for rate determining step determination. Slope value for SPCE + str., SPCE + str. + apt., and SPCE + str. + apt. + spike was 0.52, 0.48, and 0.42, respectively. The values indicate the diffusion-controlled electrochemical reaction, which could be caused by diffusion of electroactive species to the electrode surface through the biomolecules bonded on the electrode surface.

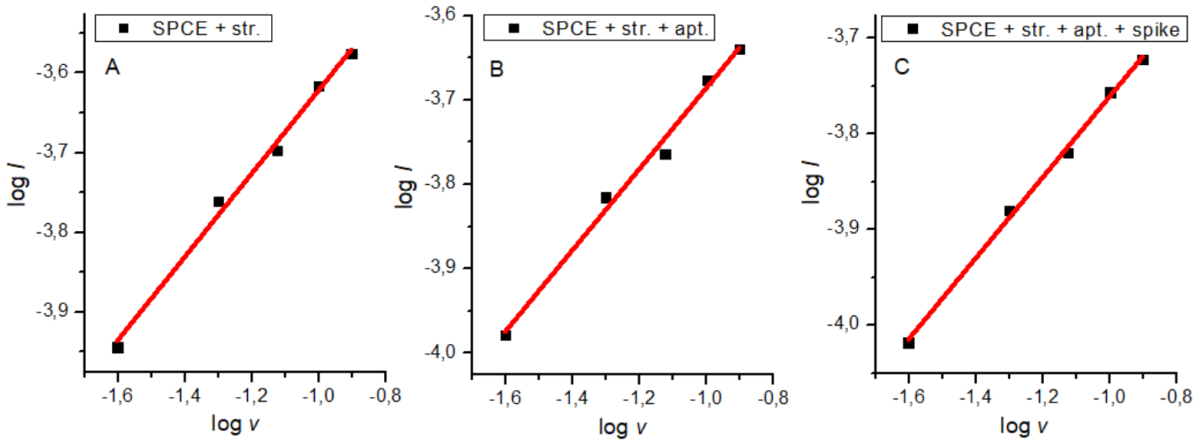

Fig. 2: Linear dependences of log *I* on log *v* for different modification of SPCE electrodes (SPCE + str. (A), SPCE + str. + apt. (B), and SPCE + str. + apt. + spike (C)) fitted by linear function.

Heterogeneous rate constants k^0 was calculated via Nicholson equation:

$$k^0 = \psi[\frac{(\pi\, D\, n\, v\, F)}{RT}]^{\frac{1}{2}} \qquad (1)$$

where k^0 is the standard rate constant in cm.s^{-1}; D is the diffusion coefficient in m^2.s^{-1}, n is the number of electrons exchanged in the reaction, v is the scan rate given in V.s^{-1}, Ψ is the Nicolson dimensionless number, F, π, and R has a usual meaning. The Nicolson dimensionless number was calculated based on the equation 2:

$$\psi = \frac{-0{,}6288+0{,}0021\Delta Ep}{1-0{,}017\Delta Ep} \qquad (2)$$

where the potential separation of anodic and cathodic peaks (ΔEp) is value subtracted from the CV curve. The value k^0 for various modifications were 7.4 × 10^{-2} cm.s^{-1} (SPCE + str.), 9.6 × 10^{-2} cm.s^{-1} (SPCE + str. + apt.), and 10.0 × 10^{-2} cm.s^{-1} (SPCE + str. + apt. + spike). The results of this study highlight the k^0 value, which reflects how quickly electrons transfer between an electroactive species and an electrode surface. If the k^0 value is between 0.3 $v^{1/2} > k^0 > 2.10^{-5}\, v^{1/2}$ cm.s^{-1}, the process is considered quasi-reversible. The conclusion corresponds to the shape and peak separation obtained from the CV curves. The scan rate increases after the modification of electrode by aptamer and spike protein. It could be expected, that after aptamer and spike protein bonding the charge transfer complex is created, so the electron transfer through the electrode material is enhanced.

Acknowledgements

This research was sponsored by the NATO Science for Peace and Security Programme under grant id. G6106.

References

[1] A. Gowri, N. A. Kumar a B. S. S. Anand, "Recent advances in nanomaterials based biosensors for point of care (PoC) diagnosis of Covid-19 – A minireview," *TrAC Trends in Analytical Chemistry*, vol. 137, no 116205, April 2021, doi: 10.1016/J.TRAC.2021.116205.

[2] Z. Rahmati, M. Roushani, H. Hosseini, H. Choobin, "Label-free electrochemical aptasensor for rapid detection of SARS-CoV-2 spike glycoprotein based on the composite of $Cu(OH)_2$ nanorodes arrays as a high-performance surface substrate," *Bioelectrochemistry*, vol. 146, pp. 108106, August 2022, doi: 10.1016/j.bioelechem.2022.108106.

[3] J. Shepa, I. Šišoláková, M. Panigaj, D. Bilá, P. Jarčuška, R. Oriňaková, "Electrochemical Biosensors for Soluble Epidemal Growth Factor Receptor Detection," *Electrocatalysis*, vol. 13, no. 5, pp. 513-523, May 2022, doi.org/10.1007/s12678-022-00740-8.

[4] Z. Masood, H. Muhammad a i. A. Tahiri, "Comparison of Different Electrochemical Methodologies for Electrode Reactions: A Case Study of Paracetamol," *Electrochem*, vol. 5, no. 1, pp. 57—69, January 2024, doi: 10.3390/electrochem5010004.

[5] N. S. Chola, S. Sreenath, B. Dave, R. K. Nagarale, "A non-fassing electroosmotic pump with sandwich of poly(2-ethylaniline)-Prussian blue nanocomposite and PVDF membrane," *Electrophoresis*, vol. 40, september 2019, doi: 10.1002/elps.201900230.

Electrochemical Detection of Ciprofloxacin Using Modified Screen-Printed Electrodes

V. Čákyová[a*], J. Shepa[a], N. Király[b], I. Šišoláková[a], P. Jarčuška[c], M. Záhornacký[c], R. Oriňaková[a,d]

[a] Department of Physical Chemistry, Faculty of Science, P. J. Šafárik University in Košice, Moyzesova 11, 041 54, Košice, Slovak republic

[b]Department of Inorganic Chemistry, Faculty of Science, P. J. Šafárik University in Košice, Moyzesova 11, 041 54, Košice, Slovak republic

[c]Department of Infectology and Travel Medicine, Faculty of Medicine, Rastislavova 43, 041 90 Košice

[d]Centre of Polymer Systems, Tomáš Baťa University in Zlín, Třída Tomáše Bati 5678, 760 01 Zlín, Czech Republic

*viktoria.cakyova@student.upjs.sk

An increasing number of patients are encountering bone defects resulting from osteoporosis, sport injuries, and accidents. These conditions represent a significant risk to human health and overall quality of life, particularly as the global population ages and the prevalence of diabetes and other illnesses rises. As a result, there has been a rise in the demand for orthopaedic implants. However, implant-related infections often lead to postoperative complications and premature implant failure, which not only increases the financial and social burden but also significantly impair the patient's quality of life, ultimately restricting the clinical use of orthopaedic implants [1].

Polymer coatings with incorporated antibiotics have been thoroughly studied as a successful solution to these issues. Biodegradable polymers function as a proficient matrix for drug delivery systems, facilitating the regulated release of active compounds via mechanisms of diffusion and polymer degradation. The duration of release can be adjusted from hours to days, depending on factors such as polymer type, coating method, thickness, and pore size [2].

Up to 60% of all prosthetic hip implant infections are caused by the Gram-positive Staphylococcus aureus and Staphylococcus epidermidis, the most common pathogens causing orthopaedic implant infections. In orthopaedic applications, ciprofloxacin (CIP) has been extensively researched and demonstrated a broad anti-Gram-positive spectrum in vitro, particularly against S. aureus and S. epidermidis. Ciprofloxacin exhibits high stability, efficiency, and a low percentage of resistant strains (25-30%). Furthermore, it is easy to entrap in the polymer networks due to its low molecular weight and relatively small size [3], [4].

To guarantee the effectiveness and safety of drug-releasing coatings, it is essential to monitor the antibiotic release profile. Monitoring and analysing the release kinetics helps maintain therapeutic levels while avoiding drug depletion or excessive local exposure, which could cause bacterial resistance or cytotoxic effects. Currently, a variety of techniques are employed for the detection of antibiotics, such as colorimetric, fluorescent, and electrochemical methods [5].

In this study, modified screen-printed carbon electrodes (SPCEs, Metrohm DropSens 11L) were utilized for the electrochemical detection of ciprofloxacin because of their compact size, affordability and simple use. The working

electrode of a SPCE was modified via drop-casting technique with 10 µL of solution consist of a metal-organic framework (MOF){[$Ga_2(H_2TCPP)(OH)_2$].5DMF.2H_2O}$_n$ post-synthetically modified by the transition metal ions (Co^{2+}/Ni^{2+}) dispersed in ethanol solution. After drying, the MOF layer was stabilized using 10 µL of a Nafion-ethanol mixture, with varying Nafion-to-ethanol ratios (1:4, 1:8, and 1:16). MOFs are crystalline materials characterized by a hierarchical porous structure, consisting of metal nodes that are coordinated with organic ligands, resulting in open three-dimensional nanostructures. Their adjustable functionalities, high surface area, and strong adsorption properties make MOFs valuable for enhancing the electrochemical performance of electrodes [6]. Furthermore, the negatively charged Nafion polymer was utilized to selectively obstruct anionic species, such as chloride (Cl^-), phosphate (PO_4^{3-}) etc., which could potentially disrupt the detection of ciprofloxacin by hindering their adsorption and minimizing their effects on the electrode surface [7]. This combined modification approach is designed to enhance both the sensitivity and selectivity of SPCE.

All electrochemical measurements were carried out under the following conditions: a potential window from 0 to 1.5 V, a scan rate of 100 mV/s. These measurements were performed using a Metrohm AUTOLAB PGSTAT302N potentiostat/galvanostat (Switzerland) equipped with a connector for the SPCE system. All experiments were carried out at atmospheric pressure and laboratory temperature. Cyclic voltammetry was then used to investigate the influence of Nafion concentration on the electrochemical detection of ciprofloxacin with three electrode configurations: SPCE-MOF (violet line), SPCE-MOF-1:8 NAFION (pink line), SPCE-MOF-1:16 NAFION (blue line) (Fig. 1). The measurements were performed in 0.8 mM ciprofloxacin solution prepared in PBS. The cyclic voltammograms displays two oxidation peaks for SPCE-MOF electrode, which indicates the two-steps electrochemical mechanism. After the Nafion addition, the current response decrease, this behaviour is caused by worst conductivity of polymer film. Among the SPCE electrodes modified by Nafion film, higher peak current displays the SPCE-MOF-1:16 NAFION electrode, because the Nafion layer was thinnest. Additionally, a shift in the peak potential and disappearance of one oxidation peak for SPCE-MOF was observed, suggesting that the presence of Nafion alters the electrode surface interactions and overall electrochemical behaviour. Based on this measurement, the SPCE-MOF-1:16 NAFION electrode modification was selected for the next measurement.

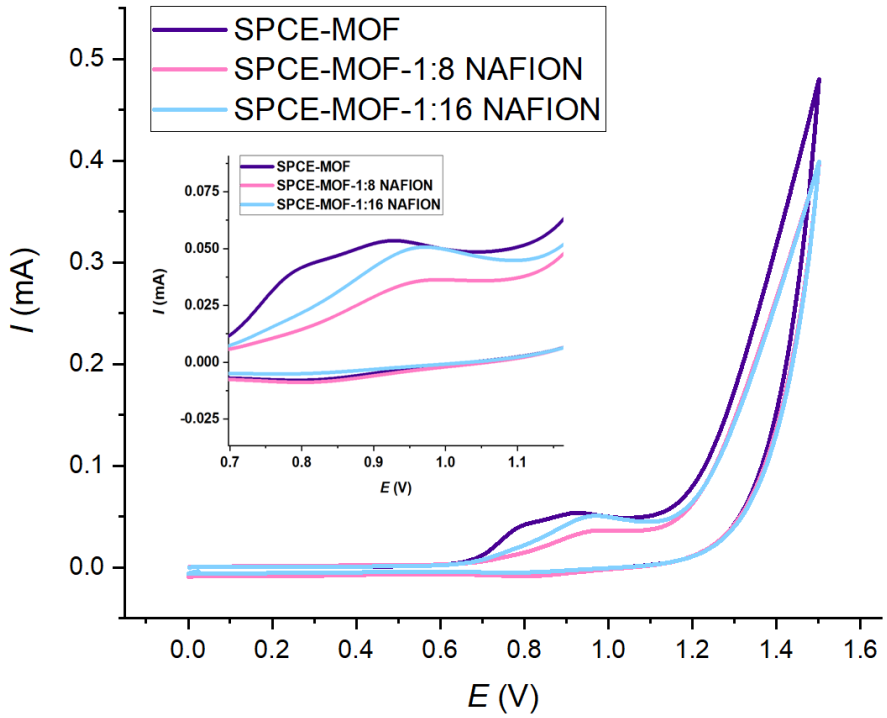

Fig. 1: Cyclic voltammograms comparing SPCE-MOF and SPCE-MOF-NAFION electrodes for ciprofloxacin analysis.

Fig. 2 A show the cyclic voltammograms of 4 ciprofloxacin concentrations (0.8, 0.6, 0.4 and 0.1 mM) in PBS at SPCE-MOF-1:16 NAFION. The dependences of peak current corresponding to ciprofloxacin oxidation and ciprofloxacin concentration were fitted by linear function (Fig. 2 B) to obtain a correlation coefficient (R^2 = 0.88).

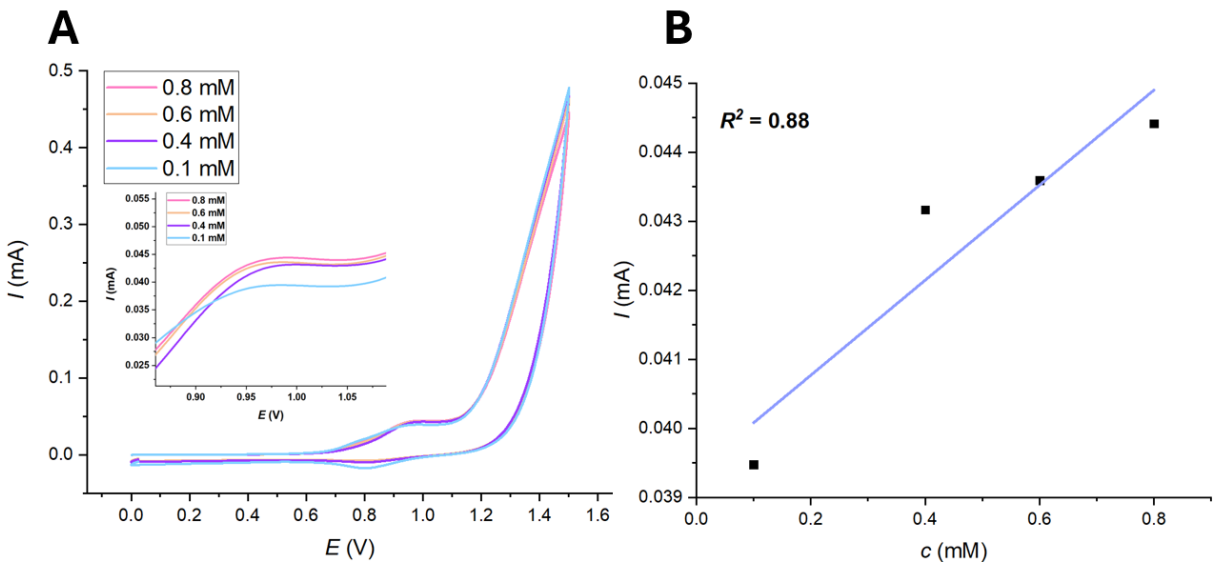

Fig. 3: Cyclic voltammogram for different ciprofloxacin concentrations (0.8, 0.6, 0.4, 0.1 mM) in PBS at SPCE-MOF-1:16 NAFION (A), calibration curve (B).

The electroanalytical characteristics of prepared SPCE-MOF-1:16 NAFION sensor were evaluated, demonstrating sensitivity of 6.89 mA/µM, and limit of detection was 413.9 µM. These findings suggest that the SPCE-MOF-1:16 NAFION sensor has potential as a rapid and direct method for ciprofloxacin detection, offering a promising approach for future antibiotic monitoring in clinical applications.

Acknowledgements

This work was funded by the EU NextGenerationEU through the Recovery and Resilience Plan for Slovakia under the project No. 09-I05-03-V02-00047.

References

[1] X. Chen, J. Zhou, Y. Qian, and L. Z. Zhao, "Antibacterial coatings on orthopedic implants", *Elsevier B.V.*, Apr. 2023, doi: 10.1016/j.mtbio.2023.100586.

[2] J. Jaworska, K. Jelonek, M. Jaworska-Kik, M. Musial-Kulik, A. Marcinkowski, J. Szewczenko, W. Kajzer, M. Pastusiak, J. Kasperczyk, "Development of antibacterial, ciprofloxacin-eluting biodegradable coatings on Ti6Al7Nb implants to prevent peri-implant infections," *J Biomed Mater Res A*, vol. 108, no. 4, pp. 1006–1015, Apr. 2020, doi: 10.1002/jbm.a.36877.

[3] A. Mehlhorn, P. Rahimi, and Y. Joseph, "Aptamer-based biosensors for antibiotic detection: A review," 2018, *MDPI*. doi: 10.3390/bios8020054.

[4] R. M. Văruț, L. T. Rotaru, D. Cimpoesu, M. Corlade, C. E. Singer, A. I. Popescu, C. Popescu, I. Iulian-Nicolae, A. Mocanu, M. Popescu, "Enhanced Antibacterial Efficacy of Bioceramic Implants Functionalized with Ciprofloxacin: An In Silico and In Vitro Study," *Pharmaceutics*, vol. 16, no. 8, Aug. 2024, doi: 10.3390/pharmaceutics16080998.

[5] S. D'Souza, "A Review of In Vitro Drug Release Test Methods for Nano-Sized Dosage Forms ," *Advances in Pharmaceutics*, vol. 2014, pp. 1–12, Nov. 2014, doi: 10.1155/2014/304757.

[6] A. D. Ambaye, K. K. Kefeni, T. G. Kebede, B. Ntsendwana, S. B. Mishra, and E. N. Nxumalo, "Cu-MOF/N-doped GO nanocomposites modified screen-printed carbon electrode towards detection of 4-nitrophenol," *Journal of Electroanalytical Chemistry*, vol. 919, Aug. 2022, doi: 10.1016/j.jelechem.2022.116542.

[7] S. Ku, S. Palanisamy, and S. M. Chen, "Highly selective dopamine electrochemical sensor based on electrochemically pretreated graphite and nafion composite modified screen printed carbon electrode," *J Colloid Interface Sci*, vol. 411, pp. 182–186, Dec. 2013, doi: 10.1016/j.jcis.2013.08.029.

Development of MOF Modified Electrochemical Sensor for Gentamicin Detection

I. Mojžišová[a]*, J. Shepa[a], N. Király [b], S. Király[a], I. Šišoláková[a], P. Jarčuška[c], M. Záhornacký[c], R. Oriňaková[a,d]

[a] Department of Physical Chemistry, Faculty of Science, P. J. Šafárik University in Košice, Moyzesova 11, 041 54, Košice

[b] Department of Inorganic Chemistry, Faculty of Science, P. J. Šafárik University in Košice, Moyzesova 11, 041 54, Košice

[c]Department of Infectology and Travel Medicine, Faculty of Medicine, Rastislavova 43, 041 90 Košice

[d] Centre of Polymer Systems, Tomáš Baťa University in Zlín, Třída Tomáše Bati 5678, 760 01 Zlín, Czech Republic

*ivana.mojzisova@student.upjs.sk

Introduction

Orthopaedic implants have revolutionized orthopaedic surgery by restoring mobility and reducing pain, significantly enhancing the quality of life for millions of people annually [1]. However, the risk of bacterial infections following surgical procedures remains a major complication. The surface of orthopaedic implants allows bacterial adhesion and colonisation, leading to bacterial biofilms, which can result in severe complications such as implant failure, osteomyelitis, arthrodesis, amputations, and, in severe cases, even death [2, 3]. For this reason, various strategies, including drug delivery systems and external assistance techniques, have been extensively explored to prevent infections associated with implants [3]. Preparing of coatings containing antibiotics shows very suitable approach, as it enables localized and controlled drug release at the implant site, ensuring optimal concentrations during critical post-surgical phases [4]. The most used antibiotics include amoxicillin, cephalexin, gentamicin, sulfamethoxazole, ciprofloxacin, and vancomycin [5], which are incorporated into implant coatings and gradually released into the implant surrounding [6]. However, it is necessary to monitor the release kinetics during coating degradation, which poses challenges, as antibiotics are released in extremely small concentrations, requiring highly sensitive analytical techniques. Traditional methods such as liquid chromatography, mass spectrometry, capillary electrophoresis, and immunoassays suffer from limitations including high costs, complex instrumentation, and bulky setups, which restrict their practicality, portability and widespread application [7]. Efforts to incorporate antibiotics into implant surfaces highlight the need for a fast, simple, efficient, and highly sensitive method for antibiotic detection. The perspective solution can be electrochemical detection with electrochemical sensors which allows speed detection, high selectivity, and cost-effectivity. However, detection using bare electrodes presents challenges such as overlapping peak potentials, limited stability, and a narrow linear range. A widely used approach to enhance detection performance is surface modification of the working electrode. Due to their exceptional porosity, large surface area, and remarkable stability, metal-organic frameworks (MOFs) are considered highly promising electrode modifiers [8]. This study focuses on the development of an electrochemical sensor for gentamicin sulphate detection, achieved by enhancing the electrode surface with a metal-organic framework (MOF).

Experiment

The screen-printed carbon electrode (SPCE 11L, Metrohm DropSens) consists of a three-electrode system, including a carbon working electrode, an Ag/AgCl pseudoreference electrode, and a carbon counter electrode, all printed on a ceramic plate. The surface of the carbon working electrode was modified with a metal-organic framework (MOF). To achieve this, 1 µl of MOF suspension in mixture of absolute ethanol: water in ration 1:1 was dropped onto the working electrode surface and left to dry in air at room temperature for 10 minutes.

Cyclic voltammetry (CV) was used to evaluate the active surface area of both unmodified and modified SPCE electrodes, as well as to conduct gentamicin determination. In both cases, measurements were performed using a potentiostat (Metrohm Autolab PGSTAT302N, Switzerland) within a potential range of 0 V to 1.5 V at a scan rate of 100 mV/s. For active surface area measurement, a 60 µl of 5 mM solution of $K_3[Fe(CN)_6]/K_4[Fe(CN)_6]$ in 1 M KCl was used.

For antibiotic detection, a 1 mM gentamicin sulfate (Genaxxon bioscience, Germany, Mw = 694.75 g/mol) solution was prepared in PBS and subsequently diluted to concentrations of 0.8 mM, 0.6 mM, 0.4 mM, 0.2 mM, and 0.1 mM. Then, 60 µl of each antibiotic concentration was dropped onto the MOF-modified working electrode and measured using CV.

Results and discussion

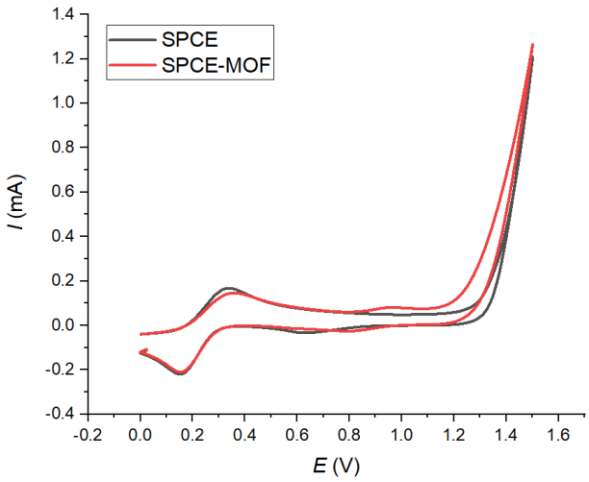

Fig. 4: Cyclic voltammograms of 5 mM $K_3[Fe(CN)_6]/K_4[Fe(CN)_6]$ in 1 M KCl at bare SPCE (black line) and SPCE modified with MOF (SPCE-MOF, red line).

Based on the acquired cyclic voltammograms of bare SPCE and SPCE modified with MOF, it can be stated that the current value in the oxidation potential region of $[Fe(CN)_6)]^{4-} \leftrightarrow [Fe(CN)_6]^{3-}$ decreased for SPCE electrode modified with MOF (SPCE-MOF) compared to the bare electrode. However, in the potential range corresponding to gentamicin

oxidation, the current response increased. The higher current values observed for SPCE-MOF indicate an enhancement in the electrochemical activity of the electrode following surface modification. MOFs possess a highly porous structure and a large surface area, providing multiple active sites that facilitate the oxidation and reduction of the analyte while also enhancing electron transport between the analyte and the electrode surface.

The size of the active surface area was calculated based on the Randles-Sevcik equation (1).

$$I_P = 0{,}4463nFAc\sqrt{\frac{nFvD}{RT}} \qquad (1)$$

According to the calculations, the active surface area of the unmodified electrode was 2.06 mm², while that of the SPE-MOF electrode was 1.8 mm².

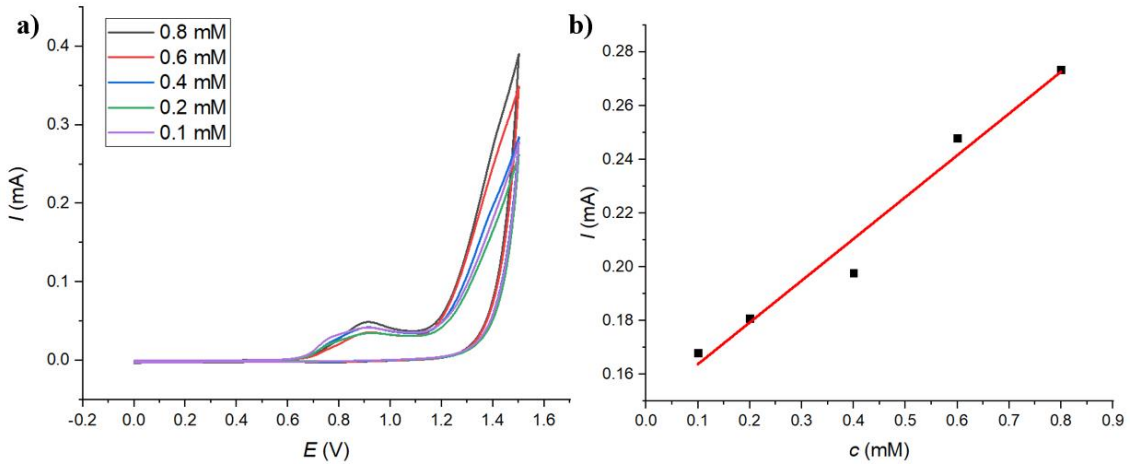

Fig. 5: a) Cyclic voltammograms of different concentrations of gentamicin in PBS solution measured with SPCE-MOF b) Dependence of current value at the potential 1.4 V on individual concentrations of gentamicin.

Fig. 2 a) shows the cyclic voltammograms for electrochemical determination of gentamicin with different concentrations by SPCE-MOF. From acquired voltammograms, the linear dependence of the current value at the same potential of 1.4 V for individual concentrations was plotted (Fig. 2 b). According to this dependence, the limit of detection (LOD) is 0.14 mM and selectivity is 0.155 mA/mM with linear range from 0.1 mM to 0.8 mM. The correlation coefficient value is R2 = 0.96.

The surface modification of the SPCE electrode with MOF led to increase in the current response (above the potential 0.6 V) compared to the unmodified electrode, enhancing its electrochemical activity. Additionally, SPCE-MOF

exhibits excellent analytical properties, making it very promising method for preparing electrodes intended for gentamicin detection.

Acknowledgements

This work was funded by the EU NextGenerationEU through the Recovery and Resilience Plan for Slovakia under the project No. 09-I05-03-V02-00047.

References

[1] M. Gimeno, P. Pinczowski, M. Pérez, A. Giorello, M. Á. Martínez, J. Santamaría, M. Arruebo, L. Luján, "A controlled antibiotic release system to prevent orthopedic-implant associated infections: An in vitro study," *European Journal of Pharmaceutics and Biopharmaceutics*, vol. 96, pp. 264–271, Oct. 2015, doi: 10.1016/J.EJPB.2015.08.007.

[2] N. J. Hickok and I. M. Shapiro, "Immobilized antibiotics to prevent orthopaedic implant infections," *Adv Drug Deliv Rev*, vol. 64, no. 12, pp. 1165–1176, Sep. 2012, doi: 10.1016/J.ADDR.2012.03.015.

[3] M. Wang, M. Wang (1), Y. Zheng, C. Yin, S. Dai, X. Fan, Y. Jiang, X. Liu, J. Fang, B. Yi, Q. Zhou, Recent Progress in Antibacterial Hydrogel Coatings for Targeting Biofilm to Prevent Orthopedic Implant-Associated Infections, *Frontiers Media SA.*, 2023, doi: 10.3389/fmicb.2023.1343202.

[4] C. Pan, Z. Zhou, and X. Yu, "Coatings as the useful drug delivery system for the prevention of implant-related infections," *J Orthop Surg Res*, vol. 13, no. 1, Sep. 2018, doi: 10.1186/s13018-018-0930-y.

[5] I. Hornyák, E. Madácsi, P. Kalugyer, G. Vácz, D. B. Horváthy, M. Szendrői, W. Han, Z. Lacza, "Increased release time of antibiotics from bone allografts through a novel biodegradable coating," *Biomed Res Int*, vol. 2014, 2014, doi: 10.1155/2014/459867.

[6]X. Chen, J. Zhou, Y. Qian, and L. Z. Zhao, "Antibacterial coatings on orthopedic implants," Apr. 01, 2023, *Elsevier B.V.* doi: 10.1016/j.mtbio.2023.100586.

[7] M. Frigoli, M.P. Krupa, G. Hooyberghs, J. W. Lowdon, T. J. Cleij, H. Diliën, K. Eersels, B. van Grinsven, "Electrochemical Sensors for Antibiotic Detection: A Focused Review with a Brief Overview of Commercial Technologies," *Multidisciplinary Digital Publishing Institute (MDPI).*, Sep. 2024, doi: 10.3390/s24175576.

[8] J. Zhao, Y. Kan, Z. Chen, H. Li, and W. Zhang, "MOFs-Modified Electrochemical Sensors and the Application in the Detection of Opioids," *MDPI.*, Feb. 2023, doi: 10.3390/bios13020284.

Morphology and Composition Analysis of a Novel High-Entropy Alloy

M. Paračková[a]*, R. Oriňaková[a], M. Strečková[b], A. Gubóová[b]

[a] Department of Physical Chemistry, Institute of Chemistry, Faculty of Science, Pavol Jozef Šafárik University in Košice, Moyzesova 11, 040 01 Košice, Slovak Republic

[b] Institute of Materials Research, Slovak Academy of Sciences, Watsonova 47, 040 01 Košice, Slovak Republic

* maria.parackova@student.upjs.sk

The discovery of new materials has played a crucial role in human development throughout history, driving significant societal shifts from the Stone Age to the modern era [1]. In 2004, a novel class of materials known as high-entropy alloys (HEAs) emerged. HEAs are composed of at least five principal elements, each with an atomic percentage ranging from 5% to 35%. They exhibit many attractive properties, such as excellent strength, high thermostability and corrosion resistance. These unique characteristics make HEAs promising candidates for various applications. As a result, research on HEAs has expanded rapidly since their discovery [2, 3, 4].

This study investigates morphology and elemental composition of a novel high-entropy alloy synthesized using ammonia solution, citric acid, and five metal salts: $Cu(NO_3)_2 \cdot 3H_2O$; $Fe(NO_3)_3 \cdot 9H_2O$; $Ni(NO_3)_2 \cdot 6H_2O$; $(NH_4)_6Mo_7O_{24} \cdot 4H_2O$; $Zn(NO_3)_2 \cdot 6H_2O$. The alloy was prepared via the sol-gel method followed by heat treatment. Its morphology and composition were analysed by scanning electron microscopy (SEM) equipped with an energy-dispersive X-ray (EDX) detector.

As shown in the SEM image at 1,000× magnification (Fig. 1A), the prepared material consists of flake-like fragments of irregular sizes and shapes. Most of these fragments exhibit a porous structure, which is a result of gas release during the combustion process. The SEM image in Fig. 1B provides a closer view, revealing that the surfaces of these flakes are covered with spherical nanoparticles approximately 20–50 nm in size.

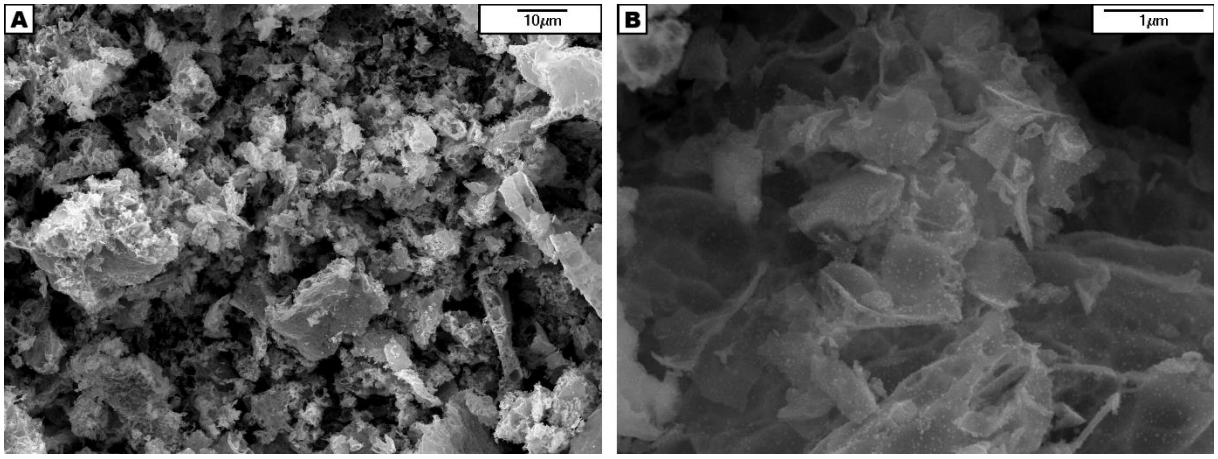

Fig. 1: SEM images of prepared high-entropy alloy taken at A) 1,000× and B) 20,000× magnification.

Regarding elemental composition, EDX analysis confirmed the formation of HEA, as the concentration of each element falls within the 5–35 atomic percentage range (Fig. 2).

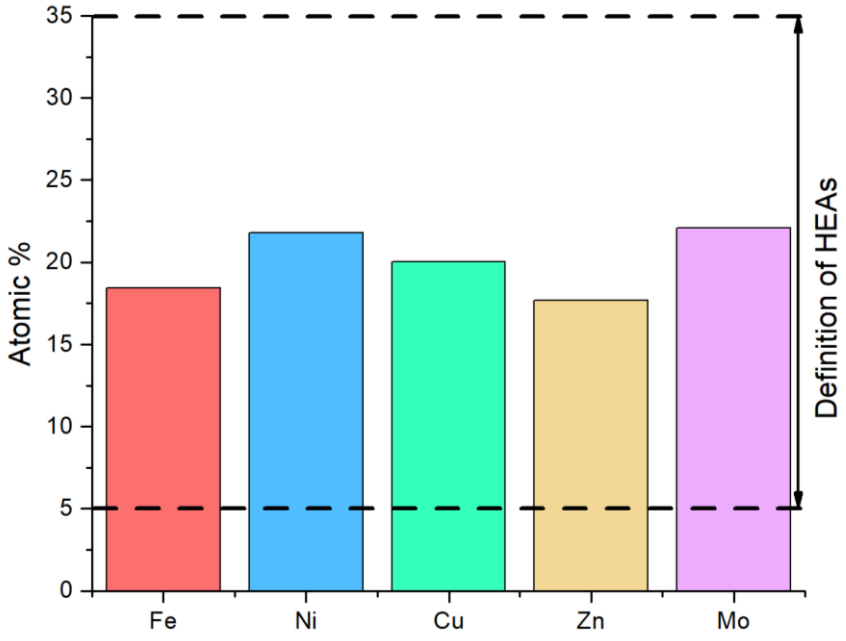

Fig. 6: Elemental composition of prepared material.

Acknowledgements

This research was supported by Slovak Research and Development Agency under the project No. APVV-20-0299, the Scientific Grant Agency of Ministry of Education, Science, Research and Sport of the Slovak Republic and the Slovak Academy of Sciences (VEGA) under project No. 1/0057/25 and Internal Scientific Grant System - ESGD Program of Pavol Jozef Šafárik University in Košice (vvgs-2023-2957) funded by the EU NextGenerationEU through the Recovery and Resilience Plan for Slovakia under the project No. 09I03-03-V05-00008.

References

[1] C. Chen, D.T. Nguyen, S. J. Lee, N. A. Baker, A. S. Karakoti, L. Lauw, C. Owen, K. T. Mueller, B. A. Bilodeau, V. Murugesan, "Accelerating Computational Materials Discovery with Machine Learning and Cloud High-Performance Computing: from Large-Scale Screening to Experimental Validation," *J Am Chem Soc*, vol. 146, no. 29, pp. 20009–20018, Jul. 2024, doi: 10.1021/jacs.4c03849.

[2] X. Wang, W. Guo, and Y. Fu, "High-entropy alloys: emerging materials for advanced functional applications," *J Mater Chem A Mater*, vol. 9, no. 2, pp. 663–701, 2021, doi: 10.1039/D0TA09601F.

[3] D. Li, C. Liu, S. Tao, J. Cai, B. Zhong, J. Li, W. Deng, H. Hou, G. Zou, X. Ji, "High-Entropy Electrode Materials: Synthesis, Properties and Outlook," *Nanomicro Lett*, vol. 17, no. 1, Dec. 2025, doi: 10.1007/s40820-024-01504-3.

[4] Z. Shi, L. Wang, Y. Huang, X. Y. Kong, and L. Ye, "High-entropy catalysts: new opportunities toward excellent catalytic activities," Sep. 06, 2023, *Royal Society of Chemistry*. doi: 10.1039/d3qm00638g.

Effect of Conductive Polymer to Active Surface Area of Potential Cholesterol Sensor

F. Chovancová[a]*, I. Šišoláková[a]

[a]Department of Physical Chemistry, Faculty of Science, Pavol Jozef Šafárik University, Moyzesova 11, 04011 Košice, Slovak Republic

*frederika.chovancova1@student.upjs.sk

The realm of electrochemical applications is progressively embracing the use of advanced polymer materials, particularly conductive polymers (CPs), due to their distinct physicochemical and electrochemical traits. CPs offer several benefits, such as lightweight construction, mechanical flexibility, scalability, and inherent corrosion resistance [1,2]. Their ability to undergo specific functionalisation makes them highly effective for sensor development. Compared to non-conductive polymers, CPs provide greater cost-efficiency, adjustable electrical properties, high environmental stability, straightforward synthesis, and opportunities for innovative uses [1,3]. These polymers feature a conjugated π-electron system, where delocalized electrons promote efficient charge movement. Moreover, CPs significantly increase the active surface area of sensors, leading to better analytical characteristics like sensitivity and selectivity. The electrical conductivity of CPs can be fine-tuned through doping techniques and polymer chain functionalization, optimizing their electrochemical characteristics. Nonetheless, the conductivity is not sensitive to fluctuations in temperature and pH, making precise environmental control essential for reliable sensor functionality. Among CPs, polypyrrole (PPy) stands out as an extensively studied option, for its excellent electrical conductivity, biocompatibility, and ease of polymerization [4].

Screen-printed electrodes are commercially produced and have found extensive application in novel electrochemical sensors development. This is attributed to the diverse range of working electrode (WE) materials, compact design, variety of working electrode shapes, and distinctive integrated multi-sensor setups. The trend of screen-printed electrodes is expanding globally [5,6].

Electrochemical sensors have shown a potential to detect disease-associated biomolecule - cholesterol. Cholesterol is an essential molecule of the human body. It plays a vital role in producing cell membranes, various hormones, and vitamin D. The physiological cholesterol level in human blood is about 300 mg/dL or 5.17 mM. Currently, a global health report suggests an increase in a number of patients with hypercholesterolemia (high level of cholesterol), which could be related to a change in lifestyle or genetic predisposition. Conventional clinical techniques to diagnose hypercholesterolemia are spectroscopic methods. Unfortunately, these methods face several problems like the pretreatment of samples, long-time analysis, and expensive laboratory equipment. Based on these problems, electrochemical sensors show the potential to overcome these problems [7,8,9]. Electrochemical sensors offered notable benefits, such as compactness, real-time monitoring, portability, high sensitivity, quick response times, low detection limits (LOD), operational simplicity, and cost-effectiveness. Incorporating CPs into electrochemical sensors continues to propel the field forward, facilitating the creation of highly selective and efficient sensing solutions for biomedical, environmental, and industrial needs [5,10,11] .

In this study, we aimed to investigate the effect of applying CP to the SPCE surface on current response and electrode surface area. SPCEs were modified by electrochemical polymerization via cyclic voltammetry (CV) method when 0.1 M pyrrole was diluted in 0.1 M sulfuric acid (H_2SO_4) as a protonation element [12]. Electrodes were polymerized via CV at a potential window ranging from -0.3 V to +1.2 V with a scan rate of 0.1 V/s for 1 cycle. To evaluate the current responses of the different types of electrodes, CV and chronoamperometry (CA) were used. Electrochemical measurements were realized in a solution consisting of 5 mM $K_4[Fe(CN)_6]/K_3[Fe(CN)_6]$ in 0.1 M KCl as a supporting electrolyte.

The results of an experiment using CV are shown in Fig. 1. The modification of electrodes increased current response from an initial value of 0.11 mA for bare SPCE to a significantly higher value of 0.23 mA for the PPy modified electrode (PPy_SPCE). The Randles-Šefčik equation (Eq. 1) was employed to calculate the active surface areas of both the bare and PPy_SPCE.

$$i_p = 0.4463nFAc\sqrt{\frac{nFvD}{RT}} \quad (1)[13]$$

Where i_p is maximum current response (A), n represents number of exchange electrons, F,R represent Farraday (C/mol) and gas constants (J/K/mol), respectively and, A is electrochemical surface of working electrode (cm^2), c is concentration of electroactive species (mol/cm^3), v is scan rate (V/s), D is diffusion coefficient (cm^2/s) and T is temperature (K).

Based on the obtained results, the active surface area of bare SPCE was calculated to be 0.11 cm^2, along with PPy_SPCE of 0.21 cm^2. This clearly represents that a modification of SPCE using CP enhanced the current response and effectively increased the active surface area of SPCE.

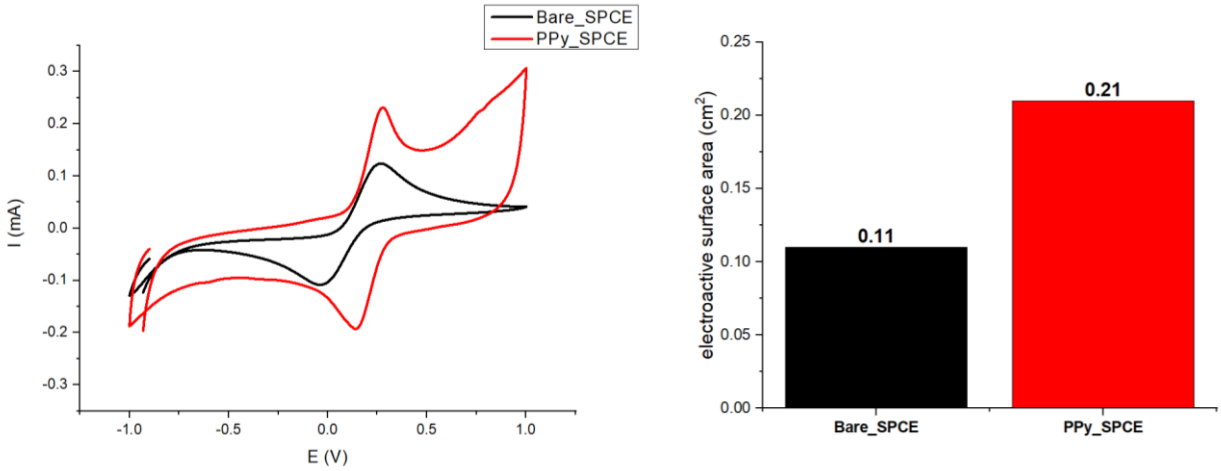

Fig. 7: Cyclic voltammogram of Bare_SPCE (black) and modified PPy_SPCE (red) in 5 mM $K_4[Fe(CN)_6]/K_3[Fe(CN)_6]$ in a supporting electrolyte of 0.1M KCl. Potential window from -1V to 1 V at scan rate of 0.1 V/s (Left). Comparison of calculated electroactive surface areas (Right).

CV and CA are commonly used to detect the electroactive surface area. CA measures the current response over time. The active surface area of the electrodes was determined through the CA for both bare SPCE and the PPy_SPCE. The duration of the experiment was set to 50 seconds to ensure comprehensive data collection, and the electroactive solution utilized remained consistent with prior experiments to maintain the integrity of the results. For the calculation of the electroactive surface area were obtained via the well-established Cottrell equation (Eq.2)

$$i = \frac{nFAc\sqrt{D}}{\sqrt{t\pi}} \qquad (2)[14]$$

where i is the current (A), n is a number of exchange electrons, F represents the Farraday constant (C/mol), A is the electrochemical surface area (cm^2), c is the concentration of electroactive species (mol/cm^3), D is diffusion coefficient (cm^2/s) and t is time (s).

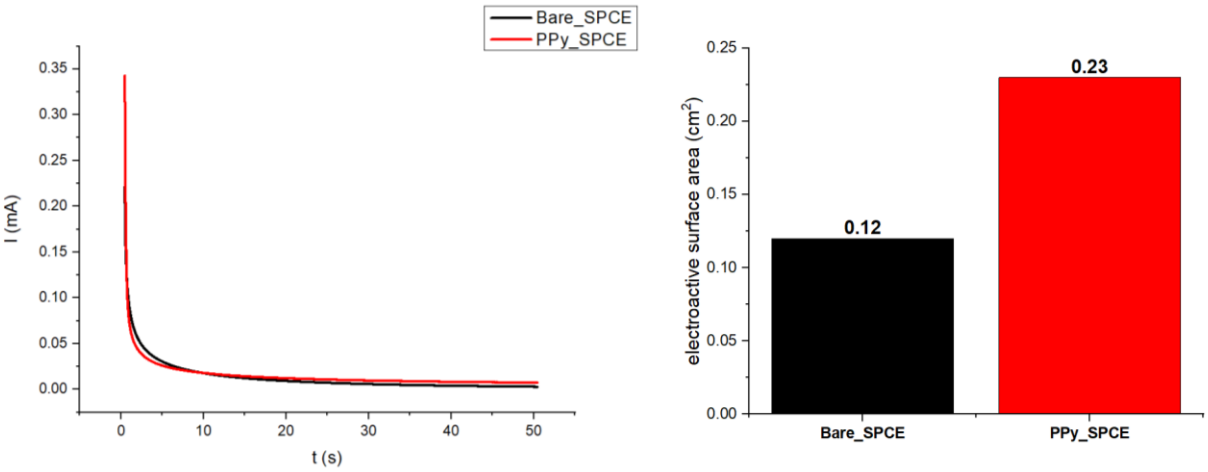

Fig. 8: Chronoamperometric response to 5 mM $K_4[Fe(CN)_6]/K_3[Fe(CN)_6]$ at potential 0.23 V in a supporting electrolyte of 0.1 M KCl on bare SPCE (black) and modified PPy_SPCE (red) (Left). Comparison of calculated electroactive surface areas (Right).

The analysis of the results derived from CA experimental data revealed that the current response for bare SPCE was 0.22 mA, while for PPy_SPCE, it was significantly higher 0.35 mA. The active surface area calculated according to the Cottrel equation (Eq. 2) of bare SPCE was determined to be 0.12 cm², whereas the active surface area of PPy_SPCE was calculated as 0.23 cm².

This notable improvement represents the modification of SPCE has significantly enhanced the current response and increased the active surface area.

Acknowledgements

Funded by the EU NextGenerationEU through the Recovery and Resilience Plan for Slovakia under the project No. 09I03-03-V05-00008.

References

[1] F. H. Narouei, H. K. Tammandani, Y. Ghalandarzehi, N. Sabbaghi, and M. Noroozifar, "An electrochemical sensor based on conductive polymers/graphite paste electrode for simultaneous determination of dopamine, uric acid and tryptophan in biological samples," *Int. J. Electrochem. Sci.*, vol. 12, no. 8, pp. 7739–7753, 2017, doi: 10.20964/2017.08.50.

[2] Z. M. Png, M. H. Chua, Q. Zhu, and J. Xu, "Conjugated polymers for electrochromic applications," in *Conjugated Polymers for Next-Generation Applications*, vol. 1*:* Synthesis, Properties and Optoelectrochemical Devices, Elsevier, 2022, pp. 539–573. doi: 10.1016/B978-0-12-823442-6.00004-0.

[3] A. Dube, S. J. Malode, A. N. Alodhayb, K. Mondal, and N. P. Shetti, "Conducting polymer-based electrochemical sensors: Progress, challenges, and future perspectives," *Talanta Open*, vol. 11, no. December 2024, p. 100395, 2025, doi: 10.1016/j.talo.2024.100395.

[4] G. Kaur, A. E. Toppo, Garima, S. K. Mehta, and S. Sharma, "Synthesis of polypyrrole (PPY) functionalized halloysite nanotubes (HNTs): An electrochemical sensor for ibuprofen," *Appl Surf Sci*, vol. 652, Apr. 2024, doi: 10.1016/j.apsusc.2023.159280.

[5] A. M. Musa, J. Kiely, R. Luxton, and K. C. Honeychurch, "Recent progress in screen-printed electrochemical sensors and biosensors for the detection of estrogens," *TrAC*, vol. 139, p. 116254, Jun. 2021, doi: 10.1016/j.trac.2021.116254.

[6] P. Karthika, S. Shanmuganathan, V. Subramanian, and C. Delerue-Matos, "Selective detection of salivary cortisol using screen-printed electrode coated with molecularly imprinted polymer," *Talanta*, vol. 272, May 2024, doi: 10.1016/j.talanta.2024.125823.

[7] O. Domínguez-Renedo, A. M. Navarro-Cuñado, and M. A. Alonso-Lomillo, "Electrochemical devices for cholesterol detection," *J Pharm Biomed Anal*, vol. 224, no. November 2022, 2023, doi: 10.1016/j.jpba.2022.115195.

[8] H. M. Yadav, J. D. Park, H. C. Kang, and J. J. Lee, "Recent development in nanomaterial-based electrochemical sensors for cholesterol detection," *Multidisciplinary Digital Publishing Institute (MDPI)* May 01, 2021, doi: 10.3390/chemosensors9050098.

[9] K. Pramanik, P. Sarkar, D. Bhattacharyay, and P. Majumdar, "One Step Electrode Fabrication for Direct Electron Transfer Cholesterol Biosensor Based on Composite of Polypyrrole, Green Reduced Graphene Oxide and Cholesterol Oxidase," *Electroanalysis*, vol. 30, no. 11, pp. 2719–2730, Nov. 2018, doi: 10.1002/elan.201800318.

[10] Y. Liu and G. Dykstra, "Recent progress on electrochemical (bio)sensors based on aptamer-molecularly imprinted polymer dual recognition," *Sensors and Actuators Reports*, vol. 4, Nov. 2022, doi: 10.1016/j.snr.2022.100112.

[11] S. Shrivastava, N. Jadon, and R. Jain, "Next-generation polymer nanocomposite-based electrochemical sensors and biosensors: A review," Sep. 01, 2016, *Elsevier B.V.* doi: 10.1016/j.trac.2016.04.005.

[12] R. Ivanov, C. Czibula, C. Teichert, M. Bojinov, and V. Tsakova, "Carbon screen-printed electrodes for substrate-assisted electroless deposition of palladium," *Journal of Electroanalytical Chemistry*, vol. 897, no. March, p. 115617, 2021, doi: 10.1016/j.jelechem.2021.115617.

[13] I. Šišoláková, R. Gorejová, F. Chovancová, J. Shepa, F.A. Nqwabebhoh, A.F. Straková, P. Sáha, R. Orińaková, "Polymer-based Electrochemical Sensor: Fast, Accurate, and Simple Insulin Diagnostics Tool," *Electrocatalysis*, no. 0123456789, 2023, doi: 10.1007/s12678-023-00827-w.

[14] I. Šišoláková, J. Hovancova, R. Orińaková, A. Orin, D. R. Garcia, O. Shylenko, and J. Radońák, "Comparison of Insulin Determination on NiNPs / chitosan-MWCNTs and NiONPs / chitosan-MWCNTs Modified Pencil Graphite Electrode," pp. 1–11, 2018, doi: 10.1002/elan.201800483.

Effect of Partial Infiltration of Metal Foams With Polyamide 6 on the Mechanical Properties

W. Du[a]*, I. N. Orbulov[a,b], P. Tamás-Bényei[c,d,e], C. Wiener[a,b], ,

aDepartment of Materials Science and Engineering, Budapest University of Technology and Economics, Műegyetem rkp. 3., H-1111 Budapest, Hungary

bMTA–BME Lendület "Momentum" High-performance Composite Metal Foams Research Group, Műegyetem rakpart 3., H-1111 Budapest, Hungary

cDepartment of Polymer Engineering, Budapest University of Technology and Economics, Műegyetem rkp. 3., H-1111 Budapest, Hungary

d HUN-REN-BME Research Group for Composite Science and Technology, Műegyetem rkp. 3, H-1111 Budapest, Hungary

e MTA-BME Lendület Sustainable Polymers Research Group, Műegyetem rkp. 3, H-1111 Budapest, Hungary

*duwanrong@edu.bme.hu

Abstract

The paper proposes to use hot-pressing method to partially infiltrate the open-cell aluminum foam with polyamide 6 (PA6). The produced PA6-AlSi12 foam exhibit higher strength, specific flexural strength and stiffness compared to the AlSi12 foam. The mechanical behavior of the metal foam and the PA6-AlSi12 foam hybrid structure was studied using the three-point bending test. The analysis of the fracture surface revealed that the crack propagation takes place mostly at the metal-PA6 interface in the hybrid structure.

1 Introduction

Due to their unique structure, metal foams has a range of advantageous properties, such as high strength-to-weight ratio, good energy and excellent sound absorption capabilities [1, 2]. Because of these properties, metal foams are often used as the core material in sandwich panels. Typically, a foam sandwich panel is a sandwich structure composed of either metal or composite material as the face sheets and a foam core [3].

The application of new core and face sheets materials has led to the widespread use of sandwich panels. Sandwich structures have the advantage of light weight, high strength and stiffness [4]. The mechanical properties of sandwich panels depend on strength of face sheets and core materials, and the bonding strength at the interfaces. In practical applications, sandwich panels usually need to bear various loads, such as bending load, impact load, and shear load [5]. The three-point bending test [6] can comprehensively evaluate the flexural strength, stiffness, and interface bonding performance of the sandwich panel, providing key data support for material optimization, structural design, and engineering applications, but delamination issues remain major challenges. The delamination phenomenon [7] is mainly caused by poor interface bonding between the face sheets and the core material or interface damage caused by long-term external force.

In this study, in order to solve the delamination problem, polyamide 6 (PA6) was infiltrated into the open-cell metal foam. Yuan et al. [8] and Chaturvedi et al. [9] have already studied the polymer-metal hybrid structures. However, in order to produce a low-weight material, we fabricated a sandwich structure by controlling the PA-infiltration depth of the metal foam.

2 Materials and methods

2.1 Materials

Polyamide 6 granules (A. Schulman, Inc., USA.) and AlSi12 were selected to produce sandwich panels. The chemical composition of AlSi12 matrix is given in Tab. 1.

Tab. 1 Chemical composition of AlSi12 matrix material

Element	Al	Si	Fe	Cu	Mg	Mn	Ni	Zn	Sn	Other
Weight %	bal.	10.5~13.5	< 0.10	< 0.1	< 0.05	< 0.55	< 0.05	< 0.15	< 0.05	< 0.05

The salt replication process was used to produce open-cell foam. First, sodium chloride particles with a 3-4 mm size as a template were prepared. The sieved salt particles were placed into a steel mold and sintered at a temperature of 800 °C for 2 hours to achieve an interconnected structure.

AlSi12 alloy was melted in an induction furnace, while the salt template was preheated to 400 °C. The salt particles were infiltrated with the molten Al alloy at a pressure of 5 bar using argon gas. After cooling down the metal to room temperature, panels of 20 mm in thickness were cut from the block.

Finally, the panels were immersed in water to leach out the salt particles. Through this process, AlSi12 metal foam with an open cell structure was obtained with 49% ± 0.02 porosity.

Polymer-metal foam hybrid was produced using the hot-pressing method. First, PA6 sheets of 5 mm thickness were made to achieve an approximately 90% of infiltration of the metal foam with PA6. The PA sheets were made from the PA6 granules. The PA6 granules were first dried at 80 °C for 24 hours to remove moisture. Subsequently, they were hot pressed at 235°C for 5 minutes, and then cooled for 10 minutes. Then, the prepared PA6 sheets were hot-pressed into the top and bottom of the foam panel at 240°C and 150 bar to make the hybrid structure.

2.2 Methods

A Zwick Z020 tester machine was used to carry out the three-point bending test at room temperature with a cross-head speed of 5 mm/min. The loading head and the supports were steel cylinders with a diameter of 10 mm and the span was 40 mm. The nominal size of the samples was 20 mm x 20 mm x 74 mm.

The cross-section of the polymer-metal foam hybrid structure and the fracture surface after the bending test were investigated by an Olympus SZX16 stereo microscope and ZEISS EVO MA 10 scanning electron microscope (SEM), respectively.

The density of each sample was calculated as the ratio of mass to volume. The volume was obtained by measuring the length, width and thickness of the sample with a caliper.

3 Results and discussion

3.1 Structural characterization

The cross-section of the polymer-metal foam hybrid is shown in Fig. 1. It can be seen that the applied hot-press manufacturing method is capable of producing polymer-metal foam hybrid structure, however, the intended sandwich-structure is only successfully achived on one side of the sample.

As Fig. 1 shows, the PA6 has infiltrated into the core foam of the structure, and the infiltration depth is uneven. The average depth of PA6 in the hybrid panels is 9.17 ± 2.48 mm, measured in 25 points on four surfaces. The average density of the foam and the hybrid structure were 1.36 ± 0.05 g/cm^3 and 1.48 ± 0.06 g/cm^3 as shown in Tab. 2. After the PA6 infiltrates the foam, part of the pores are filled, thus increasing the overall density. The high variation of the PA6 infiltration depth can be related to the highly inhomogeneous internal structure of the open-cell foam or to the uneven heat distribution of the plates during the hot pressing process. Besides local changed in the metal foam's density, it is also the reason for the difference in density between PA6 infiltrated samples.

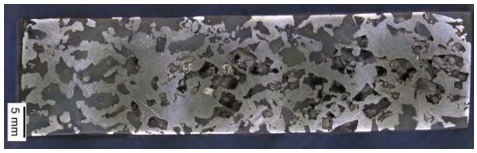

Fig. 1 PA6 – AlSi12 foam hybrid sructure under 0.7x magnification

Tab. 2 Parameters of the AlSi12 foam and the hybrid structure (90% PA6 infiltrated AlSi12 foam)

sample	length (mm)	width (mm)	thickness (mm)	weigth (g)	density (g/cm^3)
pure foam-1	73.5	20.61	19.16	40.44	1.39
pure foam-2	73.28	20.43	18.96	37.41	1.32
90% infilrated-1	73.14	19.23	19.79	40.06	1.44

90% infilrated-2	73.69	20.34	19.72	44.91	1.52

3.2 Mechanical properties

Fig. 2 shows the load-deflaction curves recorded during the 3-point bending test. The maximum bending force endured by the 90% PA6 infiltrated hybrid panel is significantly higher than the metal foam without PA6 material. This result shows that the infiltration of PA6 significantly enhances the flexural strength of the material. Specifically, the hybrid panel with PA6 had a higher load-bearing capacity under the same deflection conditions. This shows that by infiltrating the metal foam with PA6, the structure becomes stiffer and stronger. Tab. 3 shows that PA6 infiltration significantly improves the flexural strength of the foam, enhances its load-bearing capacity and mechanical properties. PA6 infiltration also improves the specific flexural strength, but the specific flexural strength of 90% infiltrated-1 is higher than that of 90% infiltrated-2, which may be due to the uneven distribution of PA6 inside the AlSi12 foam.

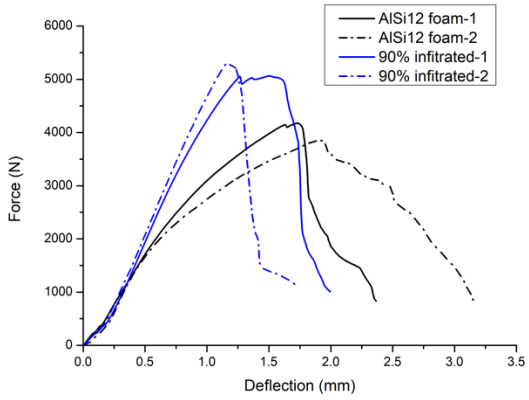

Fig. 2 The load-deflection curves, black: AlSi12 foam, blue: PA6 infiltrated AlSi12 foam

Tab. 3 Parameters of the density, flexural strength, and specific flexural strength of hybrid panels with pure foam core material and 50% PA6 infiltration depth

sample	density g/cm^3	flexural strength MPa	specific flexural strength MPa/(g/cm^3)
pure foam-1	1.39	27.21	23.76
pure foam-2	1.32	29.83	23.88
90% infilrated-1	1.44	40.32	28.02
90% infilrated-2	1.52	40.30	26.52

3.3 Fracture analysis

The SEM images of fracture surface of samples after the bending test are shown in Fig. 3. Fig. 3 (a) and (b) both show the characteristics of brittle fracture. Fig. 3 (a) exhibits the cleavage fracture of the silicon phase; Fig. 3 (b) occurs at the interface between PA6 and metal, and its fracture surface is smooth.

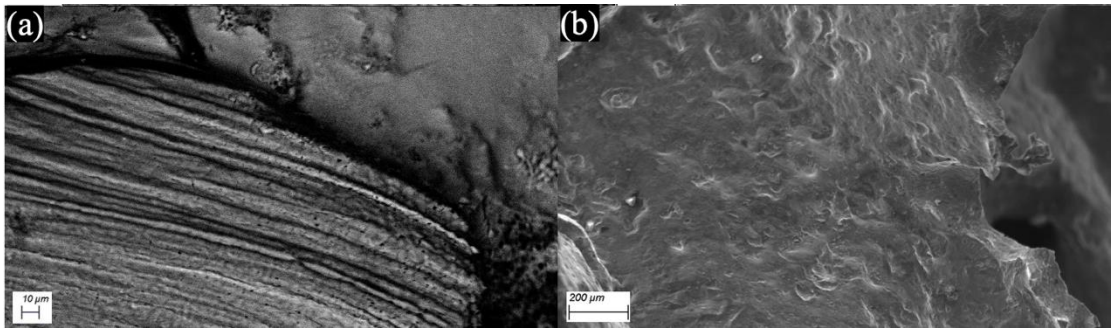

Fig. 3 SEM micrographs of the fracture surface of AlSi12 open-cell foam sample (a), and sandwich panel with infiltrated PA6 sample (b) after three-point bending test

4 Conclusion

Metal foam sandwich panels with 90% PA6 infiltrated were successfully manufactured by a hot-pressing method. Three-point bending tests show that the PA-infiltrated significantly improves the stiffness and the strength of the panel. SEM micrographs show that in the case of the hybrid structure, the interface between the metal foam core and the infiltrated PA6 is not good, and thus, the fracture propagates at the interface of the metal and the PA.

Acknowledgements

This work was supported by the National Research, Development and Innovation Office (NKFIH), under grant agreement OTKA-FK_21 138505.

References

[1] N. Khaire, M. Gupta, and G. Tiwari, “Blast resistance of graded aluminium foam core sandwich structure against blast loading,” *Materials Today: Proceedings,* vol. 87, pp. 159-163, 2023.

[2] H. Guo, and J. Zhang, “Expansion of sandwich tubes with metal foam core under axial compression,” *Journal of Applied Mechanics,* vol. 90, no. 5, pp. 051008, 2023.

[3] S. S. Marchese, G. Epasto, V. Crupi, and Y. Garbatov, “Feasibility study on additive-manufactured honeycomb sandwich structural solutions for a Fast Patrol Vessel,” *Composite Structures,* vol. 351, pp. 118607, 2025.

[4] B. V. Ramnath, K. Alagarraja, and C. Elanchezhian, “Review on sandwich composite and their applications,” *Materials Today: Proceedings,* vol. 16, pp. 859-864, 2019.

[5] R. Naik, S. Panda, and V. Racherla, “A new method for joining metal and polymer sheets in sandwich panels for highly improved interface strength,” *Composite Structures,* vol. 251, pp. 112661, 2020.

[6] F. Xia, Y. Durandet, P. Tan, and D. Ruan, “Three-point bending performance of sandwich panels with various types of cores,” *Thin-Walled Structures*, vol. 179, pp. 109723, 2022.

[7] S. Sridharan (Ed.), *Delamination behaviour of composites* Woodhead Publishing, Abington Hall, Granta Park, Great Abington, Cambridge, CB21 6AH, UK

[8] Z. Yuan, N. Rayess, and N. Dukhan, “Modeling of the mechanical properties of a polymer-metal foam hybrid,” *Procedia Materials Science*, vol. 4, pp. 215-219, 2014.

[9] A. Chaturvedi, “Recent developments in the field of metal foam-polymer hybrid materials: A brief overview,” *Journal of Metals, Materials and Minerals,* vol. 28, no. 1, pp. 136-140, 2018.

International meeting on advanced materials

Book of Abstracts

Edited by: Mgr. Soňa Király

Publisher: Pavol Jozef Šafárik University in Košice
ŠafárikPress Publishing

Year: 2025
Pages: 67
Author's heets: 4,20
Edition: first

ISBN 978-80-574-0396-8 (e-publication)